Solid-State ^{91}Zr NMR Spectroscopy Studies of Zirconocene Olefin Polymerization Catalyst Precursors

Aaron J. Rossini,[†] Ivan Hung,[†,§] Samuel A. Johnson,[†] Carla Slebodnick,[‡] Mike Mensch,[‡] Paul A. Deck,[‡] and Robert W. Schurko*,[†]

Department of Chemistry and Biochemistry, University of Windsor, Windsor, Ontario, Canada N9B 3P4, and Department of Chemistry, Virginia Polytechnic Institute and State University, Blacksburg, Virginia 24061-0121, United States

Received August 27, 2010; E-mail: rschurko@uwindsor.ca

Abstract: ^{91}Zr ($I = 5/2$) solid-state NMR (SSNMR) spectra of the zirconocene compounds, Cp_2ZrCl_2, $Cp^*_2ZrCl_2$ (**1**), Cp_2ZrBr_2 (**2**), $(Me_3SiC_5H_4)_2ZrBr_2$ (**3**), $O(Me_2SiC_5H_4)_2ZrBr_2$ (**4**), $(1,3-C_5H_3)(SiMe_2OSiMe_2)_2(1,3-C_5H_3)ZrBr_2$ (**5**), Ind_2ZrCl_2 (**6**), $Cp_2ZrMeCl$ (**7**), Cp_2ZrMe_2 (**8**), and $[Cp_2ZrMe][MeB(C_6F_5)_3]$ (**9**) have been acquired. Static ^{91}Zr SSNMR spectra have been acquired for all complexes at magnetic fields of 9.4 and 21.1 T. Cp_2ZrCl_2 and complexes **1** to **5** possess relatively narrow central transition powder patterns which allows for magic-angle spinning (MAS) ^{91}Zr solid-state NMR spectra to be acquired at a moderate field strength of 9.4 T. Complexes **6** to **9** possess ultrawideline central transition SSNMR spectra necessitating piece-wise acquisition techniques. From the static and MAS ^{91}Zr SSNMR spectra, it is possible to measure ^{91}Zr electric field gradient (EFG) and chemical shift (CS) tensor parameters, as well as the Euler angles which describe their relative orientation. Basis sets and methods for the accurate quantum chemical calculation of ^{91}Zr EFG and CS tensors have been identified. The origin of the observed EFG and CS tensor parameters are further investigated by visualization of the EFG and CS tensor orientations within the molecular frames. Correlations between the observed and calculated NMR tensor parameters and molecular symmetry and structure are made. All of these observations suggest that ^{91}Zr SSNMR spectroscopy can be utilized to probe the molecular structure of a variety of homogeneous and heterogeneous olefin polymerization catalysts.

Introduction

Cyclopentadienyl (Cp) transition metal complexes (metallocenes) have found increasing use as both homogeneous and heterogeneous olefin polymerization catalysts in industrial processes over the last 15 to 20 years.[1−5] Metallocene catalysts offer several advantages over the traditional heterogeneous Ziegler−Natta[6−9] (i.e., $TiCl_4$ supported on $MgCl_2$) and Philips[7,10,11] (i.e., CrO_x supported on

SiO_2) catalysts, such as generally higher polymerization activities and resultant polymers with narrow molecular weight distributions and potentially higher molecular weights. The tacticity of the resulting polymers can also be easily controlled via judicious alteration of the Cp ligand framework.[2,5,12,13] All of these advantages can be attributed to the "single site" nature of the metallocene catalysts, standing in stark contrast to the heterogeneous Ziegler−Natta and Philips catalysts, which possess several different active surface sites that give rise to correspondingly nonuniform polymers. In particular, zirconium metallocene derivatives (zirconocenes) have probably attracted the most research interest due to their practical properties, which include stability at conventional polymerization temperatures, low relative cost of materials, and high catalytic activities.[5]

For most industrial processes heterogeneous catalysts are preferred. For this reason, metallocenes and other organometallic catalysts are frequently immobilized onto inorganic support materials (e.g., SiO_2, $MgCl_2$, Al_2O_3). A cocatalyst, usually methylaluminoxane (MAO), may be contacted with the support before or after immobilization of the metallocene.[3,4] However, the insolubility and disordered nature of the surface-supported metallocene precatalysts and cocatalysts prevent characterization by standard techniques, such as X-ray diffraction (XRD) and

[†] Department of Chemistry and Biochemistry, University of Windsor.
[‡] Department of Chemistry, Virginia Polytechnic Institute and State University.
[§] Current Address: Center of Interdisciplinary Magnetic Resonance, National High Magnetic Field Laboratory, 1800 East Paul Dirac Drive, Tallahassee, Florida 32310, United States.

(1) Soga, K. *Macromol. Symp.* **1996**, *101*, 281–288.
(2) Coates, G. W. *J. Chem. Soc.-Dalton Trans.* **2002**, (4), 467–475.
(3) Hlatky, G. G. *Chem. Rev.* **2000**, *100* (4), 1347–1376.
(4) Severn, J. R.; Chadwick, J. C.; Duchateau, R.; Friederichs, N. *Chem. Rev.* **2005**, *105* (11), 4073–4147.
(5) Janiak, C., Metallocene Catalysts for Olefin Polymerization. In *Metallocenes: Synthesis, Reactivity, Applications*, Togni, A., Halterman, R. L., Eds.; Wiley-VCH Verlag GmbH: Weinheim, 1998; Vol. 2, pp 547–623.
(6) Bohm, L. L. *Angew. Chem., Int. Ed.* **2003**, *42* (41), 5010–5030.
(7) Zecchina, A.; Groppo, E.; Bordiga, S. *Chem.−Eur. J.* **2007**, *13* (9), 2440–2460.
(8) Soga, K.; Shiono, T. *Prog. Polym. Sci.* **1997**, *22* (7), 1503–1546.
(9) Kim, S. H.; Somorjai, G. A. *Proc. Natl. Acad. Sci. U.S.A.* **2006**, *103* (42), 15289–15294.
(10) Zecchina, A.; Lamberti, C.; Bordiga, S.; Spoto, G.; Zecchina, A. *Chem. Rev.* **2005**, *105* (1), 115–183.
(11) Theopold, K. H. *Eur. J. Inorg. Chem.* **1998**, *1*, 15–24.
(12) Miller, S. A.; Bercaw, J. E. *Organometallics* **2006**, *25* (15), 3576–3592.
(13) Wild, F.; Zsolnai, L.; Huttner, G.; Brintzinger, H. H. *J. Organomet. Chem.* **1982**, *232* (3), 233–247.

solution NMR spectroscopy. Classical surface chemistry characterization techniques such as IR,[14−18] XPS,[16,19−21] and MAS ^{1}H, ^{13}C, and ^{29}Si SSNMR[15,16,18,22−28] spectroscopy have frequently been employed to study supported organometallic complexes and cocatalysts. Data obtained from these techniques have revealed that the peripheral Cp ligands remain coordinated to the metal center upon immobilization and that alkyl groups bound to the metal center may be transferred to Lewis acid sites on the support. However, there are several ambiguities regarding the interactions between the metallocene precatalyst and cocatalyst in both homogeneous and heterogeneous systems. For example, (MAO) is the preferred cocatalyst for zirconocenes in industrial olefin polymerization; however, its molecular structure remains poorly understood.[3,4,29−32] Studies by Jordan, Marks, and Rausch on dimethyl zirconocene and tris- and tetra(pentafluorophenyl)boron adducts have demonstrated that the generation of a zirconocene-cocatalyst ion pair of the form [Cp_2ZrMe^+][A^-] is required to generate an active olefin polymerization catalyst.[33−38] Solution ^{13}C and [91]Zr NMR[39,40] and solid-state ^{13}C NMR experiments[41] conducted on MAO-zirconocene adducts with low Al:M (M = Zr, Ti) ratios (ca. 5−20) have demonstrated that the reaction between metallocene dichlorides and MAO results in the formation of similar cationic zirconocenes. However, in order to obtain highly active catalysts very large MAO:zirconocene ratios are required (typically 10^2 to 10^4:1).[38,42] The catalyst structure at high MAO:zirconocene ratios also remains poorly understood.[38] Similarly, intermediate species of the type $Cp_2Zr(R)(olefin)^+$ are generally assumed to form during the polymerization process.[5,43] For all of these reasons, the development of additional tools capable of probing the structure of zirconocenes would be invaluable.

Owing to advances in hardware and pulse sequence programming, as well as the increased availability of high field NMR spectrometers, there has been a recent flurry of activity in the acquisition of SSNMR spectra of unreceptive quadrupolar nuclei[44−52] such as [91]Zr. Our group has been investigating the possibility of utilizing solid-state NMR (SSNMR) spectra of quadrupolar (nuclear spin, $I > 1/2$) metal nuclei (e.g., [47/49]Ti, [91]Zr, [93]Nb, and [139]La) in metallocenes to probe the structures and identities of a variety of metallocene species.[53−56] The SSNMR spectra of these metal nuclei have allowed us to examine the electronic environment and molecular symmetry from the perspective of the central metal atom. Additionally, we have also recently presented a [35]Cl SSNMR study of crystalline group IV metallocene chloride complexes.[57] Because of our success with these bulk crystalline systems, and the importance of zirconocenes in heterogeneous catalytic produc-

(14) Panchenko, V. N.; Danilova, I. G.; Zakharov, V. A.; Paukshtis, E. A. *Kinet. Catal.* **2004**, *45* (4), 547–553.

(15) Joubert, J.; Delbecq, F.; Sautet, P.; Le Roux, E.; Taoufik, M.; Thieuleux, C.; Blanc, F.; Coperet, C.; Thivolle-Cazat, J.; Basset, J. M. *J. Am. Chem. Soc.* **2006**, *128* (28), 9157–9169.

(16) Atiqullah, M.; Akhtar, M. N.; Faiz, M.; Moman, A.; Abu-Raqabah, A. H.; Khan, J. H.; Wazeer, M. I. *Surf. Interface Anal.* **2006**, *38* (10), 1319–1327.

(17) Panchenko, V. N.; Semikolenova, N. V.; Danilova, I. G.; Paukshtis, E. A.; Zakharov, V. A. *J. Mol. Catal. A-Chem.* **1999**, *142* (1), 27–37.

(18) Blanc, F.; Thivolle-Cazat, J.; Basset, J. M.; Coperet, C.; Hock, A. S.; Tonzetich, Z. J.; Schrock, R. R. *J. Am. Chem. Soc.* **2007**, *129* (5), 1044–1045.

(19) Bianchini, D.; dos Santos, J. H. Z.; Uozumi, T.; Sano, T. *J. Mol. Catal. A-Chem.* **2002**, *185* (1−2), 223–235.

(20) Eisen, M. S.; Marks, T. J. *J. Am. Chem. Soc.* **1992**, *114* (26), 10358–10368.

(21) Atiqullah, M.; Faiz, M.; Akhtar, M. N.; Salim, M. A.; Ahmed, S.; Khan, J. H. *Surf. Interface Anal.* **1999**, *27* (8), 728–734.

(22) Ahn, H.; Marks, T. J. *J. Am. Chem. Soc.* **2002**, *124* (24), 7103–7110.

(23) Jezequel, M.; Dufaud, V.; Ruiz-Garcia, M. J.; Carrillo-Hermosilla, F.; Neugebauer, U.; Niccolai, G. P.; Lefebvre, F.; Bayard, F.; Corker, J.; Fiddy, S.; Evans, J.; Broyer, J. P.; Malinge, J.; Basset, J. M. *J. Am. Chem. Soc.* **2001**, *123* (15), 3520–3540.

(24) Le Roux, E.; Chabanas, M.; Baudouin, A.; de Mallmann, A.; Coperet, C.; Quadrelli, E. A.; Thivolle-Cazat, J.; Basset, J. M.; Lukens, W.; Lesage, A.; Emsley, L.; Sunley, G. J. *J. Am. Chem. Soc.* **2004**, *126* (41), 13391–13399.

(25) Reven, L. *J. Mol. Catal.* **1994**, *86* (1−3), 447–447.

(26) Vasnetsov, S. A.; Nosov, A. V.; Mastikhin, V. M.; Zakharov, V. A. *J. Mol. Catal.* **1989**, *53* (1), 37–41.

(27) Blanc, F.; Basset, J. M.; Coperet, C.; Sinha, A.; Tonzetich, Z. J.; Schrock, R. R.; Solans-Monfort, X.; Clot, E.; Eisenstein, O.; Lesage, A.; Emsley, L. *J. Am. Chem. Soc.* **2008**, *130* (18), 5886–5900.

(28) Blanc, F.; Coperet, C.; Lesage, A.; Emsley, L. *Chem. Soc. Rev.* **2008**, *37* (3), 518–526.

(29) Bryant, P. L.; Butler, L. G.; Reyes, A. P.; Kuhns, P. *Solid State Nucl. Magn. Reson.* **2000**, *16* (1−2), 63–67.

(30) Negureanu, L.; Hall, R. W.; Butler, L. G.; Simeral, L. A. *J. Am. Chem. Soc.* **2006**, *128* (51), 16816–16826.

(31) Wu, F. J.; Simeral, L. S.; Mrse, A. A.; Eilertsen, J. L.; Negureanu, L.; Gan, Z. H.; Fronczek, F. R.; Hall, R. W.; Butler, L. G. *Inorg. Chem.* **2007**, *46* (1), 44–47.

(32) Stellbrink, J.; Niu, A. Z.; Allgaier, J.; Richter, D.; Koenig, B. W.; Hartmann, R.; Coates, G. W.; Fetters, L. J. *Macromolecules* **2007**, *40* (14), 4972–4981.

(33) Jordan, R. F.; Dasher, W. E.; Echols, S. F. *J. Am. Chem. Soc.* **1986**, *108* (7), 1718–1719.

(34) Jordan, R. F.; Bajgur, C. S.; Willett, R.; Scott, B. *J. Am. Chem. Soc.* **1986**, *108* (23), 7410–7411.

(35) Chien, J. C. W.; Tsai, W. M.; Rausch, M. D. *J. Am. Chem. Soc.* **1991**, *113* (22), 8570–8571.

(36) Yang, X. M.; Stern, C. L.; Marks, T. J. *J. Am. Chem. Soc.* **1991**, *113* (9), 3623–3625.

(37) Yang, X. M.; Stern, C. L.; Marks, T. J. *J. Am. Chem. Soc.* **1994**, *116* (22), 10015–10031.

(38) Chen, E. Y. X.; Marks, T. J. *Chem. Rev.* **2000**, *100* (4), 1391–1434.

(39) Tritto, I.; Li, S. X.; Sacchi, M. C.; Locatelli, P.; Zannoni, G. *Macromolecules* **1995**, *28* (15), 5358–5362.

(40) Siedle, A. R.; Lamanna, W. M.; Newmark, R. A.; Schroepfer, J. N. *J. Mol. Catal. A-Chem.* **1998**, *128* (1−3), 257–271.

(41) Sishta, C.; Hathorn, R. M.; Marks, T. J. *J. Am. Chem. Soc.* **1992**, *114* (3), 1112–1114.

(42) Babushkin, D. E.; Semikolenova, N. V.; Zakharov, V. A.; Talsi, E. P. *Macromol. Chem. Phys.* **2000**, *201* (5), 558–567.

(43) Tritto, I.; Donetti, R.; Sacchi, M. C.; Locatelli, P.; Zannoni, G. *Macromolecules* **1999**, *32* (2), 264–269.

(44) Dybowski, C.; Bal, S. *Anal. Chem.* **2008**, *80* (12), 4295–4300.

(45) Mackenzie, K. J. D.; Smith, M. E., *Multinuclear Solid-State NMR of Inorganic Materials*, 1st ed.; Pergamon: Oxford, 2002.

(46) Kentgens, A. P. M. *Geoderma* **1997**, *80* (3−4), 271–306.

(47) Lipton, A. S.; Heck, R. W.; Sears, J. A.; Ellis, P. D. *J. Magn. Reson.* **2004**, *168* (1), 66–74.

(48) Lipton, A. S.; Sears, J. A.; Ellis, P. D. *J. Magn. Reson.* **2001**, *151* (1), 48–59.

(49) Smith, M. E., Recent progress in solid-state NMR of low-gamma nuclei. In *Annual Reports on Nmr Spectroscopy*, 2001; Vol. 43, pp 121−175.

(50) Smith, M. E.; van Eck, E. R. H. *Prog. Nucl. Magn. Reson. Spectrosc.* **1999**, *34* (2), 159–201.

(51) Ashbrook, S. E.; Duer, M. J. *Concepts Magn. Reson. Part A* **2006**, *28A* (3), 183–248.

(52) *Comprehensive Organometallic Chemistry III*; Wasylishen, R. E., Bernard, G. M., III, Crabtree, R. H., Mingos, D. M. P., Parkin, G., Eds.; Elsevier: Oxford, 2007; Vol. 1, pp 451−482.

(53) Hamaed, H.; Lo, A. Y. H.; Lee, D. S.; Evans, W. J.; Schurko, R. W. *J. Am. Chem. Soc.* **2006**, *128* (39), 12638–12639.

(54) Hung, I.; Schurko, R. W. *J. Phys. Chem. B* **2004**, *108* (26), 9060–9069.

(55) Lo, A. Y. H.; Bitterwolf, T. E.; Macdonald, C. L. B.; Schurko, R. W. *J. Phys. Chem. A* **2005**, *109* (32), 7073–7087.

(56) Rossini, A. J.; Hung, I.; Schurko, R. W. *J. Phys. Chem. Lett.* **2010**, *1* (20), 2989–2998.

(57) Rossini, A. J.; Mills, R. W.; Briscoe, G. A.; Norton, E. L.; Geier, S. J.; Hung, I.; Zheng, S.; Autschbach, J.; Schurko, R. W. *J. Am. Chem. Soc.* **2009**, *131* (9), 3317–3330.

Chart 1. Schematic Representation of Compounds Which Have Been Studied by Solid-State ^{91}Zr NMR: Bis(cyclopentadienyl)zirconium Dichloride [Cp$_2$ZrCl$_2$], Bis(pentamethylcyclopentadienyl)zirconium Dichloride [Cp*$_2$ZrCl$_2$ (**1**)], Bis(cyclopentadienyl)zirconium Dibromide [Cp$_2$ZrBr$_2$ (**2**)], Bis(trimethylsilylcyclopentadienyl)zirconium Dibromide [(Me$_3$SiC$_5$H$_4$)$_2$ZrBr$_2$ (**3**)], [O(Me$_2$SiC$_5$H$_4$)$_2$ZrBr$_2$ (**4**)], [(1,3-C$_5$H$_3$)(SiMe$_2$OSiMe$_2$)$_2$(1,3-C$_5$H$_3$)ZrBr$_2$ (**5**)], Bis(indenyl)zirconium Dichloride [Ind$_2$ZrCl$_2$ (**6**)], Bis(cyclopentadienyl)methylzirconium Chloride [Cp$_2$ZrMeCl (**7**)], Bis(cyclopentadienyl)dimethylzirconium [Cp$_2$ZrMe$_2$ (**8**)], and the Active Polymerization Catalyst [Cp$_2$ZrMe][MeB(C$_6$F$_5$)$_3$] (**9**)
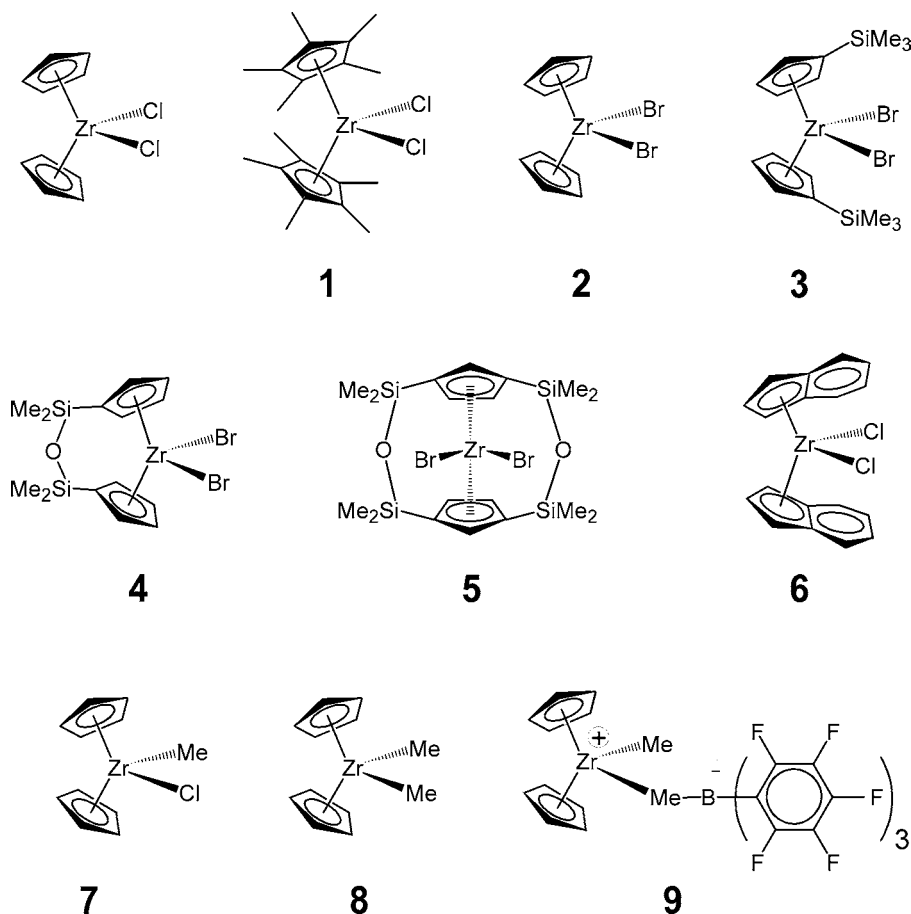
tion of polyolefins, it seems that ^{91}Zr SSNMR is a logical choice for the characterization of immobilized metallocene catalysts.

There are relatively few NMR studies of zirconium compounds in the condensed phase owing to the relatively low sensitivity of ^{91}Zr ($I = 5/2$), which has a moderate quadrupole moment ($Q(^{91}$Zr$) = -1.76(3) \times 10^{-29}$ m^2),[58] a low natural abundance (11.23%) and a relatively low magnetogyric ratio (-2.49750×10^7 rad T^{-1} s^{-1}). Previous studies have been limited to extended systems such as zirconium oxides, phosphates, silicates, and halides.[59−72] Our previous work on

Cp$_2$ZrCl$_2$ remains the only example of a molecular system studied by ^{91}Zr SSNMR.[54] Therefore, it is of importance to initially characterize model zirconocene compounds in order to correlate the structural features of metallocenes with the NMR interaction tensor parameters obtained from experimental NMR spectra. These model systems will also aid in determining the most suitable quantum chemical methods for the accurate calculation of ^{91}Zr NMR parameters, which should permit future theoretical predictions of unknown metallocene structures.

Herein, we report a comprehensive ^{91}Zr SSNMR study of a series of zirconocenes, which serve as precursors for the preparation of heterogeneous and homogeneous catalysts (compounds **1−8**, Chart 1). We have also acquired the ^{91}Zr SSNMR spectrum of an active olefin polymerization catalyst [Cp$_2$ZrMe][MeB(C$_6$F$_5$)$_3$] (**9**). These samples were examined in

(58) Kello, V.; Pyykko, P.; Sadlej, A. J.; Schwerdtfeger, P.; Thyssen, J. *Chem. Phys. Lett.* **2000**, *318* (1−3), 222–231.
(59) Bastow, T. J. *J. Phys.-Condens. Matter* **1990**, *2* (29), 6327–6330.
(60) Zhu, J. F.; Lin, Z.; Yan, Z. M.; Huang, Y. N. *Chem. Phys. Lett.* **2008**, *461* (4−6), 260–265.
(61) Yan, Z. M.; Kirby, C. W.; Huang, Y. N. *J. Phys. Chem. C* **2008**, *112* (23), 8575–8586.
(62) Armelao, L.; Gross, S.; Muller, K.; Pace, G.; Tondello, E.; Tsetsgee, O.; Zattin, A. *Chem. Mater.* **2006**, *18* (25), 6019–6030.
(63) Dajda, N.; Dixon, J. M.; Smith, M. E.; Carthey, N.; Bishop, P. T. *Phys. Rev. B* **2003**, *67* (2), 024201.
(64) Forwood, C. T.; Gibson, M. A.; Smith, M. E. *Phys. Rev. B* **1998**, *58* (6), 2988–2997.
(65) Hartmann, P.; Scheler, G. *Z. Naturfors., A: J. Phys. Sci.* **1995**, *50* (1), 90–94.
(66) Bastow, T. J.; Hobday, M. E.; Smith, M. E.; Whitfield, H. J. *Solid State Nucl. Magn. Reson.* **1994**, *3* (2), 49–57.
(67) Dec, S. F.; Davis, M. F.; Maciel, G. E.; Bronnimann, C. E.; Fitzgerald, J. J.; Han, S. S. *Inorg. Chem.* **1993**, *32* (6), 955–959.

(68) Bastow, T. J.; Smith, M. E.; Stuart, S. N. *Chem. Phys. Lett.* **1992**, *191* (1−2), 125–129.
(69) Hartman, J. S.; Koffyberg, F. P.; Ripmeester, J. A. *J. Magn. Reson.* **1991**, *91* (2), 400–404.
(70) Bastow, T. J.; Smith, M. E. *Solid State Nucl. Magn. Reson.* **1992**, *1* (4), 165–174.
(71) Pauvert, O.; Fayon, F.; Rakhmatullin, A.; Kramer, S.; Horvatic, M.; Avignant, D.; Berthier, C.; Deschamps, M.; Massiot, D.; Bessada, C. *Inorg. Chem.* **2009**, *48* (18), 8709–8717.
(72) Pauvert, O.; Zanghi, D.; Salanne, M.; Simon, C.; Rakhmatullin, A.; Matsuura, H.; Okamoto, Y.; Vivet, F.; Bessada, C. *J. Phys. Chem. B* **2010**, *114* (19), 6472–6479.

order to obtain the ^{91}Zr electric field gradient (EFG) and chemical shift (CS) tensor parameters for a diverse range of zirconocene structural motifs. Many of the samples possess very broad ^{91}Zr SSNMR spectra which are classified as ultrawideline spectra, since they cannot be acquired in single experiments and must be acquired in a piece-wise manner.[73,74] These ultrawideline spectra are acquired with the WURST-CPMG pulse sequence,[75,76] which combines the broadband excitation properties of frequency swept WURST pulses[77-79] with the S/N enhancement of QCPMG.[80,81] Extensive quantum chemical calculations of ^{91}Zr EFG and CS tensor parameters are presented herein, and are used to rationalize the origin of the observed NMR parameters and related to the molecular and electronic structures of the complexes. Quantum chemical calculations conducted with variable Zr–X (X = Cl, Me) bond lengths were performed in order to understand the large differences observed in the EFG tensors parameters of several complexes. Previous solution ^{91}Zr NMR studies have prefaced and inspired this current work.[82-87] In particular, Bühl, Hopp, von Philipsborn (BHP) and co-workers have studied compounds **1, 2, 3, 7, 8** and other compounds analogous to **4** and **5** using solution ^{91}Zr NMR and quantum chemical calculations;[84] therefore, we will often refer to their work for comparison with the results presented here.

Experimental Section

Samples. Samples of Cp_2ZrCl_2, $Cp*_2ZrCl_2$ (**1**) and Ind_2ZrCl_2 (**6**) were purchased from Strem Chemicals, Inc. and used without further purification. Samples of Cp_2ZrBr_2 (**2**), $(Me_3SiC_5H_4)_2ZrBr_2$ (**3**),[88] $O(Me_2SiC_5H_4)_2ZrBr_2$ (**4**),[88] $(O(Me_2Si)_2C_5H_3)_2ZrBr_2$ (**5**),[88] $Cp_2ZrMeCl$ (**7**),[89] Cp_2ZrMe_2 (**8**),[90] and $[Cp_2ZrMe][MeB(C_6F_5)_3]$ (**9**)[37] were synthesized according to previously published literature procedures and characterized by ^1H, ^{13}C and ^{19}F solution NMR. Detailed descriptions of synthetic procedures are provided in the Supporting Information.

Solid-State NMR Spectroscopy. NMR experiments were performed on a Varian Infinityplus NMR console with an Oxford 9.4 T wide bore magnet for which the ^{91}Zr resonance frequency (ν_0) is 37.16 MHz. Typical central transition selective 90° pulse widths of ~2.0 μs (corresponding to radio frequency fields of ~40 kHz) were employed along with pulse delays between 0.7 and 2.0 s. Between 6500 and 150 000 transients were acquired. Continuous wave ^1H decoupling was applied for most MAS and static experiments. For the acquisition of static and MAS spectra, a Hahn echo sequence with a 16-step phase cycle was employed.[81] Double frequency sweep (DFS)[91,92] or fast radio frequency amplitude modulated[93] (FAM) schemes were employed for some of the ^{91}Zr static and MAS spectra in order to provide signal enhancement and reduce experimental times at 9.4 T. For the acquisition of broad static ^{91}Zr NMR spectra the QCPMG pulse sequence[81] and WURST-QCPMG[75,76,79] pulse sequences were employed. MAS ^{91}Zr NMR spectra were typically acquired at spinning frequencies (ν_{rot}) between 10 000 and 15 000 Hz. 5.0 mm outer diameter (o.d.) ZrO_2 rotors were employed for acquisition of MAS spectra. Teflon or Delrin 5.0 mm o.d. sample tubes and shortened glass NMR tubes were used for nonspinning experiments. Zirconium chemical shifts were referenced to a concentrated dichloromethane (CH_2Cl_2) solution of Cp_2ZrCl_2 (δ_{iso} = 0.0 ppm). A complete list of experimental details can be found in the Supporting Information (Tables S1–S5).

High-field static NMR experiments were performed on a 21.1 T Bruker Avance II NMR spectrometer for which $\nu_0(^{91}Zr)$ = 83.7 MHz. Samples were placed in sealed shortened 5.0 mm or 4.0 mm o.d. glass NMR tubes or a 10 mm o.d. Teflon sample tube. Spectra were acquired on home-built 5 mm or 10 mm single channel probes or a Bruker 4 mm MAS HX probe. The Hahn echo, QCPMG or WURST-QCPMG pulse sequences were employed.

Spectral Simulations. Analytical simulations of NMR spectra were performed with the WSOLIDS software package.[94] The convention used for the specification of the chemical shift (CS) tensors is: $\delta_{11} \geq \delta_{22} \geq \delta_{33}$; $\delta_{iso} = (\delta_{11} + \delta_{22} + \delta_{33})/3$; $\Omega = \delta_{11} - \delta_{33}$; $\kappa = 3(\delta_{22} - \delta_{iso})/\Omega$. The convention used for specification of electric field gradient (EFG) tensors is as follows: $|V_{33}| \geq |V_{22}| \geq |V_{11}|$; $C_Q = eQV_{33}/h$; $\eta_Q = (V_{11} - V_{22})/V_{33}$. The Rose convention is used to describe the order and direction of Euler angle rotations, which describe the relative orientation of the EFG and CS tensors.[95,96] Uncertainties associated with the experimental NMR tensor parameters are estimated by taking the best simulation of the experimental spectra, and bidirectionally varying the individual NMR tensor parameters until the simulated spectrum is significantly different from the experimental spectrum.

Theoretical Calculations. Calculations of EFG tensors were performed using Gaussian 03[97] employing molecular coordinates for isolated molecules resolved by X-ray diffraction.[84,98,99] Atomic coordinates for **5** were obtained from a preliminary single crystal XRD structure (Table S8 of the SI). In all cases, idealized hydrogen atom positions were employed. For some calculations, "idealized" Cp ring coordinates were employed (see discussion section for details). Computations were carried out using the restricted Hartree–Fock (RHF) and hybrid density functional theory methods

(73) Massiot, D.; Farnan, I.; Gautier, N.; Trumeau, D.; Trokiner, A.; Coutures, J. P. *Solid State Nucl. Magn. Reson.* **1995**, *4* (4), 241–248.

(74) Medek, A.; Frydman, V.; Frydman, L. *J. Phys. Chem. A* **1999**, *103* (25), 4830–4835.

(75) O'Dell, L. A.; Schurko, R. W. *Chem. Phys. Lett.* **2008**, *464* (1−3), 97–102.

(76) O'Dell, L. A.; Rossini, A. J.; Schurko, R. W. *Chem. Phys. Lett.* **2009**, *468* (4−6), 330–335.

(77) Kupce, E.; Freeman, R. *J. Magn. Reson. A* **1995**, *115* (2), 273–276.

(78) Kupce, E.; Freeman, R. *J. Magn. Reson. A* **1996**, *118* (2), 299–303.

(79) Bhattacharyya, R.; Frydman, L. *J. Chem. Phys.* **2007**, *127* (19), 194503.

(80) Larsen, F. H.; Jakobsen, H. J.; Ellis, P. D.; Nielsen, N. C. *J. Magn. Reson.* **1998**, *131* (1), 144–147.

(81) Larsen, F. H.; Jakobsen, H. J.; Ellis, P. D.; Nielsen, N. C. *J. Phys. Chem. A* **1997**, *101* (46), 8597–8606.

(82) Bohme, U.; Thiele, K. H.; Rufinska, A. *Z. Anorg. Allg. Chem.* **1994**, *620* (8), 1455–1462.

(83) Benn, R.; Rufinska, A. *J. Organomet. Chem.* **1984**, *273* (3), C51–C54.

(84) Buhl, M.; Hopp, G.; vonPhilipsborn, W.; Beck, S.; Prosenc, M. H.; Rief, U.; Brintzinger, H. H. *Organometallics* **1996**, *15* (2), 778–785.

(85) Siedle, A. R.; Newmark, R. A.; Gleason, W. B.; Lamanna, W. M. *Organometallics* **1990**, *9* (4), 1290–1295.

(86) Sayer, B. G.; Hao, N.; Denes, G.; Bickley, D. G.; McGlinchey, M. J. *Inorg. Chim. Acta* **1981**, *48* (1), 53–55.

(87) Sayer, B. G.; Thompson, J. I. A.; Hao, N.; Birchall, T.; Eaton, D. R.; McGlinchey, M. J. *Inorg. Chem.* **1981**, *20* (11), 3748–3750.

(88) Deck, P. A.; Fisher, T. S.; Downey, J. S. *Organometallics* **1997**, *16* (6), 1193–1196.

(89) Hawrelak, E. J.; Deck, P. A. *Organometallics* **2004**, *23* (1), 9–11.

(90) Jantunen, K. C.; Scott, B. L.; Kiplinger, J. L. *J. Alloys Compd.* **2007**, *444*, 363–368.

(91) Iuga, D.; Schafer, H.; Verhagen, R.; Kentgens, A. P. M. *J. Magn. Reson.* **2000**, *147* (2), 192–209.

(92) Kentgens, A. P. M.; Verhagen, R. *Chem. Phys. Lett.* **1999**, *300* (3−4), 435–443.

(93) Madhu, P. K.; Goldbourt, A.; Frydman, L.; Vega, S. *J. Chem. Phys.* **2000**, *112* (5), 2377–2391.

(94) Eichele, K.; Wasylishen, R. E. *WSolids: Solid-State NMR Simulation Package*, V1.17.28; 2001.

(95) Arfken, G. *Mathematical Methods for Physicists*, 3rd ed.; Academic Press: New York, 1985.

(96) Rose, M. E. *Elementary Theory of Angular Momentum*; Wiley: New York, 1957.

(97) Frisch, M. J.; et al. *Gaussian 03, Revision B.03*; Gaussian, Inc.: Pittsburgh, PA, 2003.

(98) Repo, T.; Klinga, M.; Mutikainen, I.; Su, Y.; Leskela, M.; Polamo, M. *Acta Chem. Scand.* **1996**, *50* (12), 1116–1120.

(99) Hunter, W. E.; Hrncir, D. C.; Bynum, R. V.; Penttila, R. A.; Atwood, J. L. *Organometallics* **1983**, *2* (6), 750–755.

(B3LYP).[100−102] Several all-electron basis sets on zirconium were employed (see SI), including (17s13p9d)[103,104] contracted to [12s9p5d], with two sets of diffuse p functions[105] ($\alpha_p = 0.11323$ and 0.04108) and one diffuse d function ($\alpha_d = 0.0382$),[84] and (17s11p8d) contracted to [6s3p3d] or [12s7p4d].[103] The double-ζ basis set of Dunning was employed for Cl.[106] Additional Cl basis sets were also tested (SI). The 6-311G** basis sets included with Gaussian 03 were used for all other atoms. Calculations with all electron basis sets on Br were also attempted (see SI). These Br basis sets include (13s10p1d) contracted to [4s3p1d],[107] the triple-ζ basis set of Dunning[108] and the quadruple-ζ [11s7p4d][109] and triple-ζ [8s6p2d][104] basis sets of Ahlrich. Most basis sets were obtained from the EMSL Basis Set Exchange.[110] Quadrupolar coupling constants were converted from atomic units (a.u.) to Hz by multiplying the largest component of the EFG tensor, V_{33}, by $eQ/h \times 9.71736 \times 10^{21}$ V m^{-2}, where $Q(^{91}Zr) = -1.76(3) \times 10^{-29}$ m^2,[58] and $e = -1.602188 \times 10^{-19}$ C. The EFGShield program was used to extract Euler angles and generate EFG and CS tensor orientations from the Gaussian 03 output.[111]

X-ray Diffraction (XRD) Experiments. Detailed descriptions of all single crystal X-ray diffraction experiments are provided in the SI (Figures S1−S3). Samples for powder XRD were placed into 0.7 mm glass capillary tubes and flame-sealed. Powder XRD patterns were collected using a Bruker AXS HI-STAR system using a General Area Detector Diffractions System. The X-ray source was Cu Kα radiation (1.540598 Å) and an area detector using a 2θ range between 4.0° to 65.0° was employed. Powder XRD patterns were simulated with the PowderCell software package.[112]

Results and Discussion

MAS ^{91}Zr Solid-State NMR Spectra. MAS ^{91}Zr SSNMR spectra of Cp$_2$ZrCl$_2$ and complexes **1−5** are pictured in Figure 1. Before the spectra of individual complexes are discussed, there are several general observations to be made. Those complexes which feature coordination by unsubstituted or substituted Cp ligands (denoted as Cp′) and halogens possess relatively small ^{91}Zr quadrupolar coupling constants resulting in relatively narrow static and MAS ^{91}Zr second-order quadrupolar powder patterns (**6** being the exception, vide infra). This allows for central transition (CT) MAS ^{91}Zr SSNMR spectra of complexes **1−5** to be acquired at a moderate magnetic field strength (9.4 T) and at sample spinning speeds below 15 kHz. The ^{91}Zr EFG parameters (C_Q and η_Q) and isotropic chemical shift values (δ_{iso}) derived from simulation of these spectra are compiled in Table 1. The isotropic chemical shifts for **1−5** are in good agreement with values measured by BHP using solution
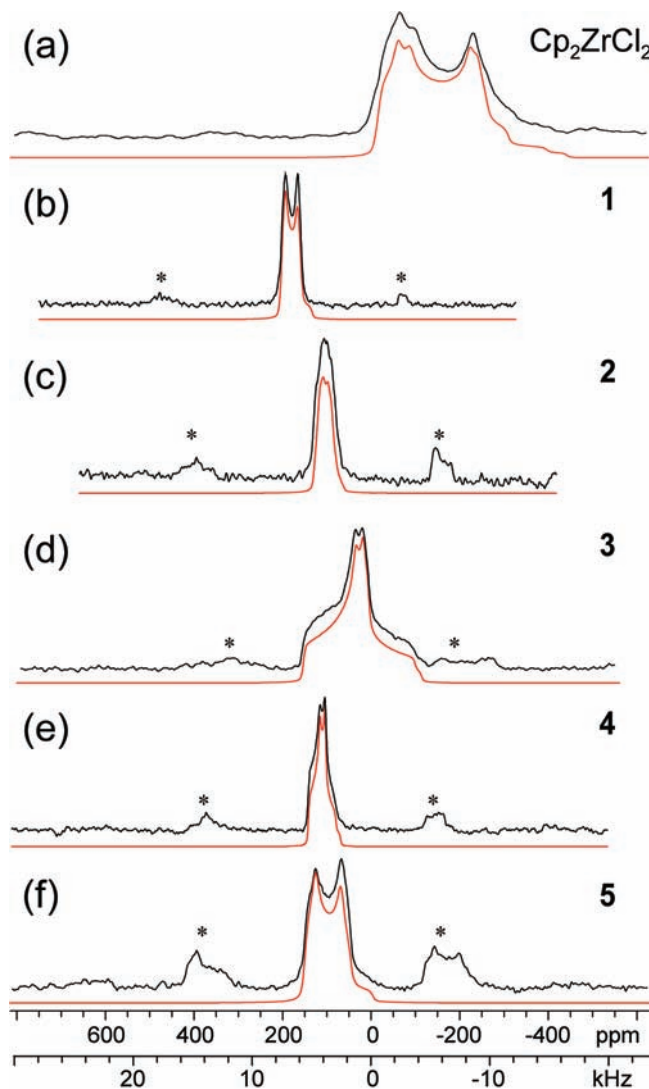
Figure 1. MAS ^{91}Zr SSNMR spectra (black traces) of (a) Cp$_2$ZrCl$_2$ at ν_{rot} = 15 000 Hz, (b) **1** [Cp*$_2$ZrCl$_2$] at ν_{rot} = 10 000 Hz, (c) **2** [Cp$_2$ZrBr$_2$] at ν_{rot} = 10 000 Hz, (d) **3** [(Me$_3$SiC$_5$H$_4$)$_2$ZrBr$_2$] at ν_{rot} = 15 500 Hz, (e) **4** [O(Me$_2$SiC$_5$H$_4$)$_2$ZrBr$_2$] at ν_{rot} = 11 000 Hz and (f) **5** [(1,3-C$_5$H$_3$)(SiMe$_2$OSiMe$_2$)$_2$(1,3-C$_5$H$_3$)ZrBr$_2$] at ν_{rot} = 10 000 Hz. Corresponding analytical simulations (red traces) are shown beneath all experimental spectra. All spectra were acquired at 9.4 T. Asterisks denote spinning sidebands.

^{91}Zr NMR.[84] It is apparent that MAS ^{91}Zr SSNMR spectra can serve as a powerful tool for identification of zirconocenes, as variations in the ring substitution, type of halide, and overall symmetry of the molecule have an obvious influence on the line shape of the spectra. In order to relate the molecular structures to the observed ^{91}Zr NMR parameters, we have compiled the average bond lengths and ligand-zirconium-ligand angles from the single crystal X-ray structures (Table 2).

We previously acquired the MAS ^{91}Zr SSNMR spectrum of Cp$_2$ZrCl$_2$ at 9.4 T.[54] For the present work, an MAS spectrum was acquired at 21.1 T in an attempt to resolve two separate signals corresponding to the two distinct sites observed in the single crystal X-ray diffraction structure.[98] The spectrum acquired at 21.1 T possesses a distinct "splitting" of the high frequency discontinuity of the CT powder pattern, indicative of the presence of two sites (Figure S4 of the SI). A simulation employing two sites yielded similar values of C_Q (6.2 and 6.5 MHz) and η_Q (0.18 and 0.30), and identical values of $\delta_{iso} = 21$

(100) Becke, A. D. *J. Chem. Phys.* **1993**, *98* (7), 5648–5652.
(101) Becke, A. D. *Phys. Rev. A* **1988**, *38* (6), 3098–3100.
(102) Lee, C. T.; Yang, W. T.; Parr, R. G. *Phys. Rev. B* **1988**, *37* (2), 785–789.
(103) Horn, H., 1991, Computational Chemistry List, Ltd. http://www.ccl.net/cca/data/basis-sets/karlsruhe-old/zr.shtml.
(104) Schafer, A.; Horn, H.; Ahlrichs, R. *J. Chem. Phys.* **1992**, *97* (4), 2571–2577.
(105) Walch, S. P.; Bauschlicher, C. W.; Nelin, C. J. *J. Chem. Phys.* **1983**, *79* (7), 3600–3602.
(106) Woon, D. E.; Dunning, T. H. *J. Chem. Phys.* **1993**, *98* (2), 1358–1371.
(107) Huzinaga, S. *Gaussian Basis Sets for Molecular Calculations*; Elsevier: New York, 1984.
(108) Wilson, A. K.; Woon, D. E.; Peterson, K. A.; Dunning, T. H. *J. Chem. Phys.* **1999**, *110* (16), 7667–7676.
(109) Weigend, F.; Furche, F.; Ahlrichs, R. *J. Chem. Phys.* **2003**, *119* (24), 12753–12762.
(110) Feller, D. *J. Comput. Chem.* **1996**, *17* (13), 1571–1586.
(111) Adiga, S.; Aebi, D.; Bryce, D. L. *Can. J. Chem.-Rev. Can. Chim.* **2007**, *85* (7–8), 496–505.
(112) Kraus, W.; Nolze, G. *PowderCell for Windows*; Federal Institute for Materials Research and Testing: Berlin, Germany, 2000.

Table 1. Experimentally Determined ^{91}Zr EFG and CS Tensor NMR Parameters[a]

compound	δ_{iso} (ppm)	$|C_Q|$ (MHz)[b]	η_Q[c]	Ω (ppm)[d]	κ[e]	α (°)	β (°)	γ (°)
Cp$_2$ZrCl$_2$ (site 1)[f]	21(5)	6.2(3)	0.18(10)	340(40)	−0.6(3)	90(35)	86(10)	2(10)
Cp$_2$ZrCl$_2$ (site 2)	21(5)	6.5(3)	0.30(10)	350(40)	−0.7(3)	90(35)	86(10)	3(10)
Cp*$_2$ZrCl$_2$ **1**	208(2)	2.6(1)	0.22(10)	235(25)	−0.75(20)	20(40)	90(25)	90(10)
Cp$_2$ZrBr$_2$ **2**[g]	125(10),132(10)	2.4(3)	0.40(20)	550(50)	−0.55(20)	40(90)	0(90)	0(90)
(Me$_3$Si−C$_5$H$_4$)$_2$ZrBr$_2$ **3**	154(5)	4.7(1)	0.88(4)					
O(Me$_2$SiC$_5$H$_4$)$_2$ZrBr$_2$ **4**	143(3)	2.5(1)	0.68(7)	620(70)	−0.8(2)	40(20)	90(15)	35(40)
(1,3-C$_5$H$_3$)(SiMe$_2$OSiMe$_2$)$_2$(1,3-C$_5$H$_3$)ZrBr$_2$ **5**	163(7)	3.9(2)	0.25(9)	530(60)	−0.55(20)	40(20)	30(15)	85(10)
Ind$_2$ZrCl$_2$ **6** (single site fit)[h]	20(50)	31.5(15)	0.33(20)	700(300)	0.6(9)	20(10)	75(15)	−40(40)
6 (two site fit, site 1)	60(50)	32.0(10)	0.25(20)	200(400)	−0.3(8)	80(60)	60(40)	4(60)
6 (two site fit, site 2)	60(50)	30.7(10)	0.38(20)	200(400)	−0.3(8)	80(60)	60(40)	4(60)
Cp$_2$ZrMeCl **7** (site 1)	230(100)	23.3(10)	0.35(10)	900(500)	−0.6(8)	5(70)	15(45)	85(70)
Cp$_2$ZrMeCl **7** (site 2)	230(100)	20.0(30)	0.75(15)	1000(500)	0.8(9)	80(40)	20(20)	5(40)
Cp$_2$ZrMe$_2$ **8**	475(40)	28.0(3)	0.40(4)	1750(300)	−0.9(3)	80(40)	90(5)	0(5)
[Cp$_2$ZrMe][MeB(C$_6$F$_5$)$_3$] **9**	350(100)	39.0(8)	0.76(6)	1000(400)	0.2(5)	90(10)	80(15)	86(40)

[a] The uncertainty in the last digit(s) of each value is denoted in brackets. [b] $C_Q = eQV_{33}/h$. [c] $\eta_Q = (V_{11} - V_{22})/V_{33}$. [d] $\Omega = \delta_{11} - \delta_{33}$. [e] $\kappa = 3(\delta_{22} - \delta_{iso})/\Omega$. [f] We have previously studied this compound by ^{91}Zr SSNMR, see ref 54. [g] Estimated parameters from overlapping sites (see text for details). [h] See text for details regarding single site and two site fits.

Table 2. Average Metrical Parameters of Single Crystal X-ray Diffraction Structures of Zirconocene Complexes[a]

compound	r(Zr-Hal) (Å)	r(Zr-Me) (Å)	∠ X-Zr-X (deg)	r(Zr-Cp′$_{Cent}$) (Å)	∠ Cp′$_{Cent}$-Zr-Cp′$_{Cent}$ (°)	ref
Cp$_2$ZrCl$_2$	2.45		97.0	2.20	129.3	98
Cp*$_2$ZrCl$_2$ **1**	2.46		95.4	2.26	130.9	113
(Me$_4$EtCp)$_2$ZrCl$_2$[b]	2.44		94.6	2.25	137.0	128
Cp$_2$ZrBr$_2$ **2**[c]	2.61		96.7	2.19	129.0	84
(Me$_3$SiC$_5$H$_4$)$_2$ZrBr$_2$ **3**	2.61		94.2	2.20	128.1	118
O(Me$_2$SiC$_5$H$_4$)$_2$ZrBr$_2$ **4**	2.61		98.0	2.20	131.2	this work
(1,3-C$_5$H$_3$)(SiMe$_2$OSiMe$_2$)$_2$(1,3-C$_5$H$_3$)ZrBr$_2$ **5**	2.60		96.7	2.19	130.4	this work
Ind$_2$ZrCl$_2$ **6**	2.44		94.7	2.23	128.3	98
Cp$_2$ZrMeCl **7**[d]	2.51	2.23	94.5	2.21	131.4	this work
Cp$_2$ZrMeCl **7**	2.49	2.36	95.1	2.21	131.1	99
Cp$_2$ZrMe$_2$ **8**		2.28	95.5	2.26	132.5	99
[Cp$_2$ZrMe][MeB(C$_6$F$_5$)$_3$] **9**[e]		2.25, 2.56	87.7	2.20	131.1	125

[a] Parameters have been taken from previously reported single crystal X-ray diffraction structures. The parameters for **4**, **5**, and **7** are taken from the structures reported in this work. [b] Quantum chemical calculations utilizing coordinates from the published crystal structure of **1** gave poor agreement with experimental NMR tensor parameters. Calculations employing atomic coordinates from (Me$_4$EtCp)$_2$ZrCl$_2$ gave much better results, therefore, we have listed the metrical parameters of this complex. [c] Conformation 2 of the second site in the asymmetric unit has been disregarded because the Cp$_{cent}$−Zr bond distance is significantly longer (2.21 Å) than the other distances in the structure. [d] The second methyl position in the asymmetric unit has been disregarded because the Zr−Me distance is abnormally short (2.176 Å). [e] The second Zr−Me distance reported corresponds to the methyl group which is bridging between the Zr and B atoms.

ppm, which is unsurprising given the similarity of the two Zr environments. The parameters obtained from the MAS spectra are similar to those previously reported by our research group.

The spectrum of **1** (Figure 1b) is characterized by a C_Q that is smaller than that of Cp$_2$ZrCl$_2$ by a factor of 2.4, a similar value of η_Q, and a δ_{iso} which is ∼180 ppm more positive. Examination of the crystal structures[98,113] of Cp$_2$ZrCl$_2$ and **1** reveals a slight lengthening in the average Zr−Cp′ centroid and Zr−Cl distances in **1** compared to Cp$_2$ZrCl$_2$, which is likely due to the steric bulk of the Cp* rings in **1**. A decrease in C_Q with lengthening of the metal−Cp′ centroid distance is consistent with observations made from variable-temperature experiments on linear sodocenes[114] and CpK.[115] BHP have also used ab initio calculations to demonstrate that the decrease in C_Q of **1** compared to Cp$_2$ZrCl$_2$ is caused largely by the electronic effects of the highly basic Cp* ligand.[84]

The MAS ^{91}Zr SSNMR spectrum of **2** (Figure 1c) appears to show the overlap of narrow patterns from two distinct zirconium species. The observation of more than one zirconium site is in

agreement with the existence of two distinct molecules in the asymmetric unit of **2**.[84] Unfortunately, the chemical shift dispersion at B_0 = 9.4 T is insufficient to resolve the nonequivalent sites of **2**, even with a high-resolution solid-state NMR technique such as triple-quantum (3Q) multiple-quantum (MQ) MAS[116,117] (Figure S5 of the SI). Nevertheless, by considering the approximate width of the pattern, it is possible to make rough estimates of the maximum C_Q, as well as δ_{iso} and η_Q. The simulation of the MAS ^{91}Zr SSNMR spectrum employs two sites which possess identical EFG tensor parameters and distinct δ_{iso} values of 125 ppm and 132 ppm. A MAS ^{91}Zr SSNMR spectrum of **2** was also acquired at 21.1 T (Figure S6 of the SI); however, even at this field, there is still insufficient resolution of the two sites. Nonetheless, these spectra still allow for the accurate determination of the EFG tensor parameters (vide infra).

The average δ_{iso} of **2** is 128.5 ppm, which is ∼100 ppm higher than that observed for Cp$_2$ZrCl$_2$. The η_Q value of **2** is similar to Cp$_2$ZrCl$_2$, while the C_Q value is ∼2.5× smaller, in accordance with the narrower ^{91}Zr solution NMR linewidths observed by BHP for **2**. The Cp−Zr bond lengths and Cp−Zr−Cp angles

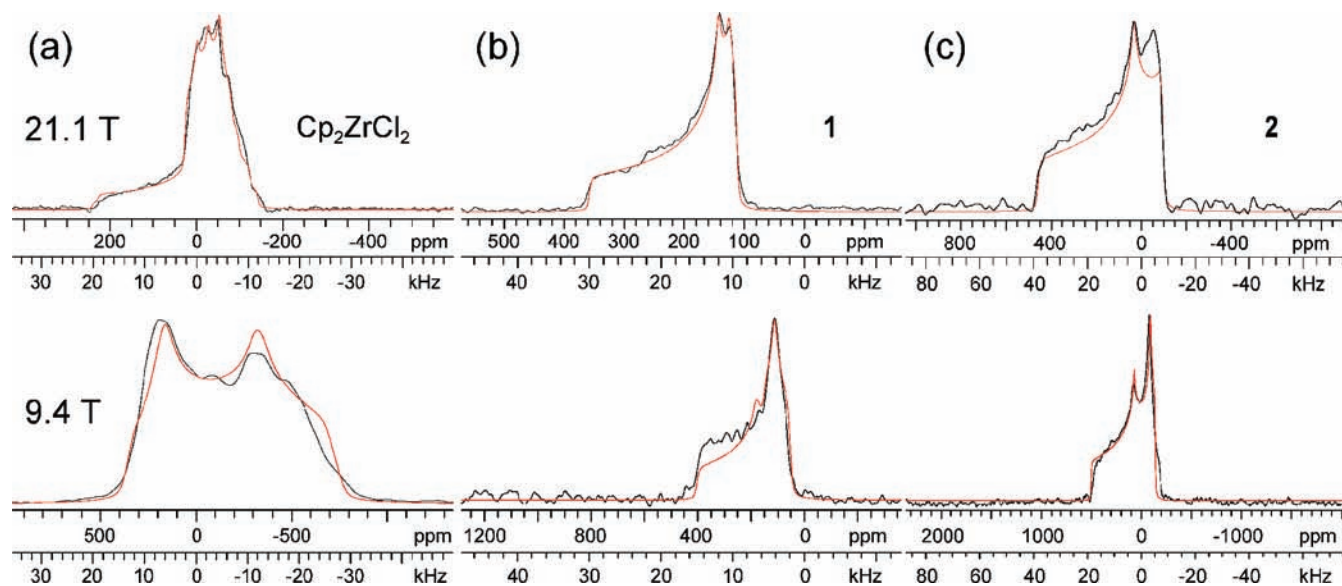(113) Bohme, U.; Rittmeister, B. Private Communication 1998, CSD Code: GEJPEQ.
(114) Willans, M. J.; Schurko, R. W. *J. Phys. Chem. B* **2003**, *107* (22), 5144−5161.
(115) Widdifield, C. M.; Schurko, R. W. *J. Phys. Chem. A* **2005**, *109* (31), 6865−6876.

(116) Medek, A.; Frydman, L. *J. Braz. Chem. Soc.* **1999**, *10* (4), 263−277.
(117) Medek, A.; Harwood, J. S.; Frydman, L. *J. Am. Chem. Soc.* **1995**, *117* (51), 12779−12787.

Figure 2. Static ^{91}Zr SSNMR spectra acquired at 9.4 T (bottom) and 21.1 T (top) of (a) Cp$_2$ZrCl$_2$, (b) **1** [Cp*$_2$ZrCl$_2$], and (c) **2** [Cp$_2$ZrBr$_2$]. Analytical simulations (red traces) which include the effects of CSA and Euler angles are overlaid on the experimental spectra.

are similar in both Cp$_2$ZrCl$_2$ and **2**, suggesting that the reduction in C_Q can be attributed to the increased lengths of Zr–Br bonds in comparison to Zr–Cl bonds (averages of 2.61 Å and 2.45 Å, respectively). This is further addressed in the quantum chemical calculation section below.

The MAS ^{91}Zr SSNMR spectra of the zirconocene dibromides, **3**, **4**, and **5** are shown in Figure 1d–f, respectively. Complex **3** has a silane moiety on the Cp rings, while **4** and **5** have *ansa*-bridging siloxane moieties on the Cp ring. The observed values of δ_{iso} are between 143 and 163 ppm, which are near the value observed for **2** (128.5 ppm). The C_Q values are larger than those observed for **2**, but smaller than that observed for Cp$_2$ZrCl$_2$. The values of η_Q are observed to be near 0 (**5**, $\eta_Q = 0.25$), intermediate (**4**, $\eta_Q = 0.68$) and near 1 (**3**, $\eta_Q = 0.88$), despite the superficial similarities in molecular structure for the three complexes, which have similar Zr-Cp′ and Zr–Br bond lengths and Cp′–Zr–Cp′ and Br–Zr–Br angles[118] (Table 2), suggesting that the differences in the EFG tensor parameters may be due to inductive effects of the various silane substituents. In this regard, Bercaw and co-workers have performed a comprehensive spectroscopic and theoretical study of *ansa*-bridged zirconocene complexes and found that the electronic structure of the Cp′-zirconium bonds can be significantly affected by *ansa* bridges.[119]

Compounds **3**, **4**, and **5** comprise a set of structures which model zirconocenes that have been tethered to a surface via reactive ancillary moieties. The conformation of **3** reflects zirconocene molecules prior to adsorption, while **4** and **5** serve as models of surface-tethered species. These results show great promise for using ^{91}Zr SSNMR for the characterization of surface-tethered zirconocenes, since (i) large changes in the substitution and conformation of the Cp′ rings, do not appear to cause large increases in C_Q, and (ii) MAS ^{91}Zr NMR spectra show sensitivity to slight changes in coordination and molecular geometry.

Static ^{91}Zr SSNMR Spectra. We have previously demonstrated that Cp$_2$ZrCl$_2$ possesses a significant ^{91}Zr chemical shift

anisotropy (CSA); hence, CSA and associated Euler angles[120−123] must be considered in simulations of static ^{91}Zr SSNMR spectra.[54] The broadening of CT powder patterns of half integer quadrupolar nuclei by the second-order quadrupolar interaction is inversely proportional to B_0, while the broadening due to CSA is directly proportional to B_0; hence, static spectra of all complexes have been acquired at two magnetic fields. Euler angles describe the relative orientation of the EFG and CS tensors; orientations of these tensors in the molecular frames have been obtained with quantum chemical calculations for all complexes, and are discussed in the following section.

The static ^{91}Zr SSNMR spectra of Cp$_2$ZrCl$_2$, **1** and **2** acquired at 9.4 and 21.1 T are shown in Figure 2. The CS tensor parameters presented herein for Cp$_2$ZrCl$_2$ are $\Omega = 340$ and 350 ppm and $\kappa = -0.60$ and -0.70, for sites 1 and 2, respectively. These parameters are slightly different from our previous values ($\Omega = 430$ ppm and $\kappa = -0.55$), due to the increased sensitivity of the spectrum acquired at 21.1 T to changes in the CS tensor parameters. The observation of κ values near -1 indicates that the distinct component of the CS tensor is δ_{11} (and that δ_{22} and δ_{33} are similar in value). κ values near -1 are observed for most of these complexes, suggesting that this is a general feature of zirconocenes.

The static spectra of **1** reveal that $\Omega = 235$ ppm and $\kappa = -0.75$. The symmetry of the CS tensor of **1** is similar to that of Cp$_2$ZrCl$_2$, as indicated by κ, however, the value of Ω is reduced. The value of δ_{iso} for **1** indicates that the Zr nucleus is significantly deshielded with respect to Cp$_2$ZrCl$_2$. The Zr–Cl distances of **1** are similar to those of Cp$_2$ZrCl$_2$, suggesting that the differences in δ_{iso} and Ω arise from the increased basicity of the Cp* ligand in comparison to the Cp ligands. The Euler

(118) Antinolo, A.; Lappert, M. F.; Singh, A.; Winterborn, D. J. W.; Engelhardt, L. M.; Raston, C. L.; White, A. H.; Carty, A. J.; Taylor, N. J. *J. Chem. Soc.-Dalton Trans.* **1987**, (6), 1463–1472.

(119) Zachmanoglou, C. E.; Docrat, A.; Bridgewater, B. M.; Parkin, G.; Brandow, C. G.; Bercaw, J. E.; Jardine, C. N.; Lyall, M.; Green, J. C.; Keister, J. B. *J. Am. Chem. Soc.* **2002**, *124* (32), 9525–9546.

(120) Cheng, J. T.; Edwards, J. C.; Ellis, P. D. *J. Phys. Chem.* **1990**, *94* (2), 553–561.

(121) Chu, P. J.; Gerstein, B. C. *J. Chem. Phys.* **1989**, *91* (4), 2081–2101.

(122) Power, W. P.; Wasylishen, R. E.; Mooibroek, S.; Pettitt, B. A.; Danchura, W. *J. Phys. Chem.* **1990**, *94* (2), 591–598.

(123) Bryce, D. L., Tensor Interplay. In *Encyclopedia of Magnetic Resonance*, Harris, R. K., Wasylishen, R. E., Eds. Wiley: New York, 2008; pp 1–11.
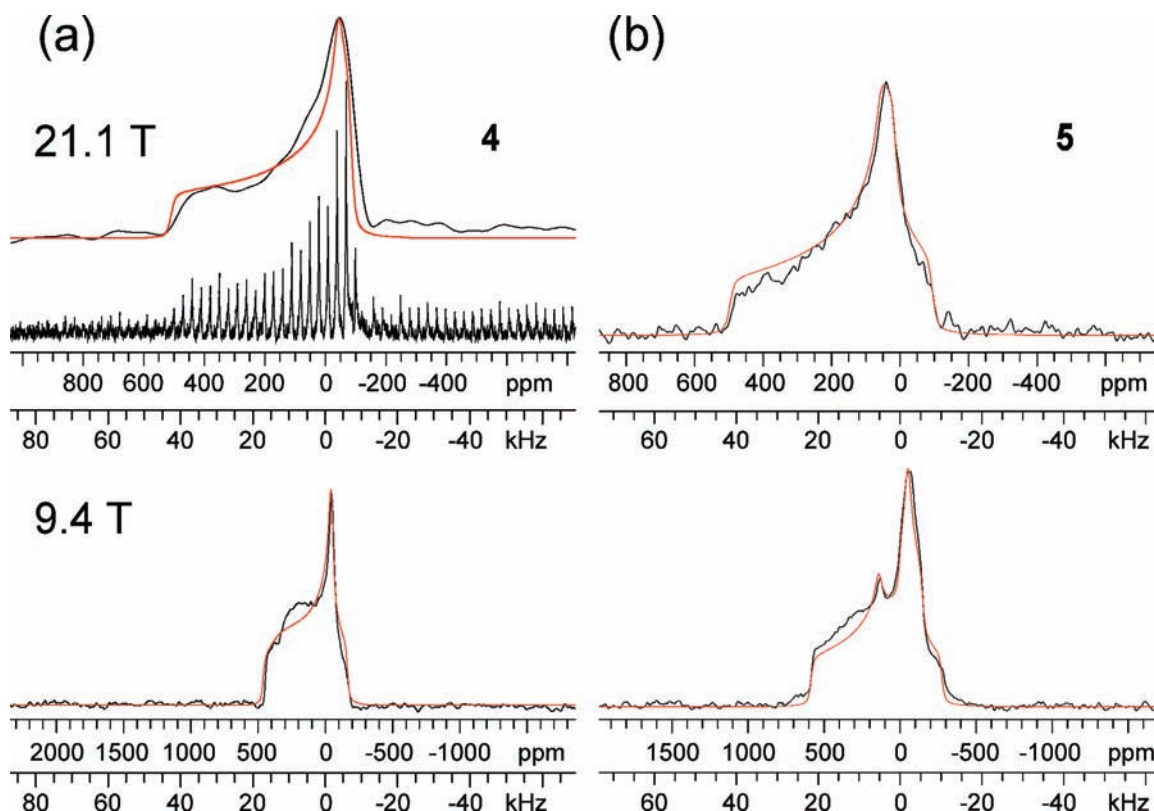
Figure 3. Static ^{91}Zr SSNMR spectra acquired at fields of 9.4 T (bottom) and 21.1 T (top) of (a) **4** [O(Me$_2$SiC$_5$H$_4$)$_2$ZrBr$_2$] and (b) **5** [(1,3-C$_5$H$_3$)(SiMe$_2$OSiMe$_2$)$_2$(1,3-C$_5$H$_3$)ZrBr$_2$]. The 21.1 T spectrum of **4** was acquired with the QCPMG sequence due to limited sample quantity. Both a spikelet spectrum and an echo spectrum resulting from coaddition of the echoes in the time domain are shown for **4**. Analytical simulations (red traces) which include the effects of CSA and Euler angles are overlaid on the experimental spectra.

angle β is near 90° for both **1** and Cp$_2$ZrCl$_2$. β describes the angle separating the largest principal component of the EFG tensor (V_{33}) and the most shielded component of the CS tensor (δ_{33}).

The static spectra of complex **2** reveals $\kappa = -0.6$, which is similar to Cp$_2$ZrCl$_2$ and **1**, but $\Omega = 550$ ppm, which is significantly larger than those of the chlorinated complexes. It is challenging to simulate the 21.1 T spectrum due to the presence of the two crystallographic sites with distinct NMR parameters. For this reason, the uncertainties in Euler angles are large; however, the breadths of the static spectra at both fields allows accurate measurements of Ω and κ to be obtained. With respect to the large zirconium CSA and small C_Q, the MAS ^{91}Zr SSNMR spectrum acquired at 21.1 T is of particular interest, possessing an extensive spinning sideband manifold not commonly observed for ^{91}Zr (Figure S6 of the SI).

The static spectra of **4** and **5** are shown in Figure 3. The values of Ω are similar to those obtained from the other brominated species, **2**. The similarity of the CS tensor parameters of **4** and **5**, taken with their distinct n_Q values and Euler angles, suggest that the EFG tensors are oriented differently within the molecular frames of these complexes. Unfortunately, static spectra of **3** could not be obtained due to limited sample quantity and sample degradation. In summary, the MAS and static ^{91}Zr spectra of Cp$_2$ZrCl$_2$ and compounds **1** through **5** suggest that the solid-state ^{91}Zr NMR spectra of brominated zirconocenes are generally characterized by more positive δ_{iso} values and larger Ω values than those of chlorinated zirconocenes, while the C_Q values are generally similar in magnitude.

In order to control the tacticity of the polymers produced by metallocene catalysts, it is necessary to alter the structure and

symmetry of the coordinating Cp ligands.[1,2,124] This is often accomplished by preparing metallocenes with modified Cp ligands such as the indenyl and fluorenyl ligands. The static ^{91}Zr NMR spectra of the bis(indenyl) complex, **6**, acquired at 9.4 and 21.1 T are shown in Figure 4. Spectra acquired at 9.4 T display significant overlap with the $^{35/37}$Cl satellite transitions,[57] making it difficult to resolve the static ^{91}Zr powder pattern at this field. This problem is lessened at 21.1 T due to a greater separation between the Larmor frequencies of $^{35/37}$Cl and ^{91}Zr. When a simulation with only a single site is employed, poor agreement with the intensities of the experimental spectrum is observed (Figure 4a). A simulation employing two sites (Figure 4b,c) results in an improved fit of the experimental spectrum and employs more realistic Ω values (200 ppm for each site). However, the previously published single crystal XRD structure shows the presence of only one magnetically distinct Zr site.[98] Solution ^{1}H and ^{13}C NMR spectroscopy confirm the sample is pure, and that the second pattern does not arise from an impurity (Figure S7 of the SI). The single crystal X-ray data was acquired at 153 K while the ^{91}Zr NMR spectra presented herein were acquired at room temperature, so it is possible that the second site is a result of polymorphism. A powder XRD pattern measured at room temperature (Figure S8 of the SI) reveals the sample is highly crystalline; however, the experimental pattern does not match that predicted from the low temperature crystal structure, confirming the possible existence of a different phase at room temperature.

Regardless of whether a one- or two-site fit is employed for **6**, a value of C_Q (>30 MHz) much larger than those observed

(124) Coates, G. W. *Chem. Rev.* **2000**, *100* (4), 1223–1252.
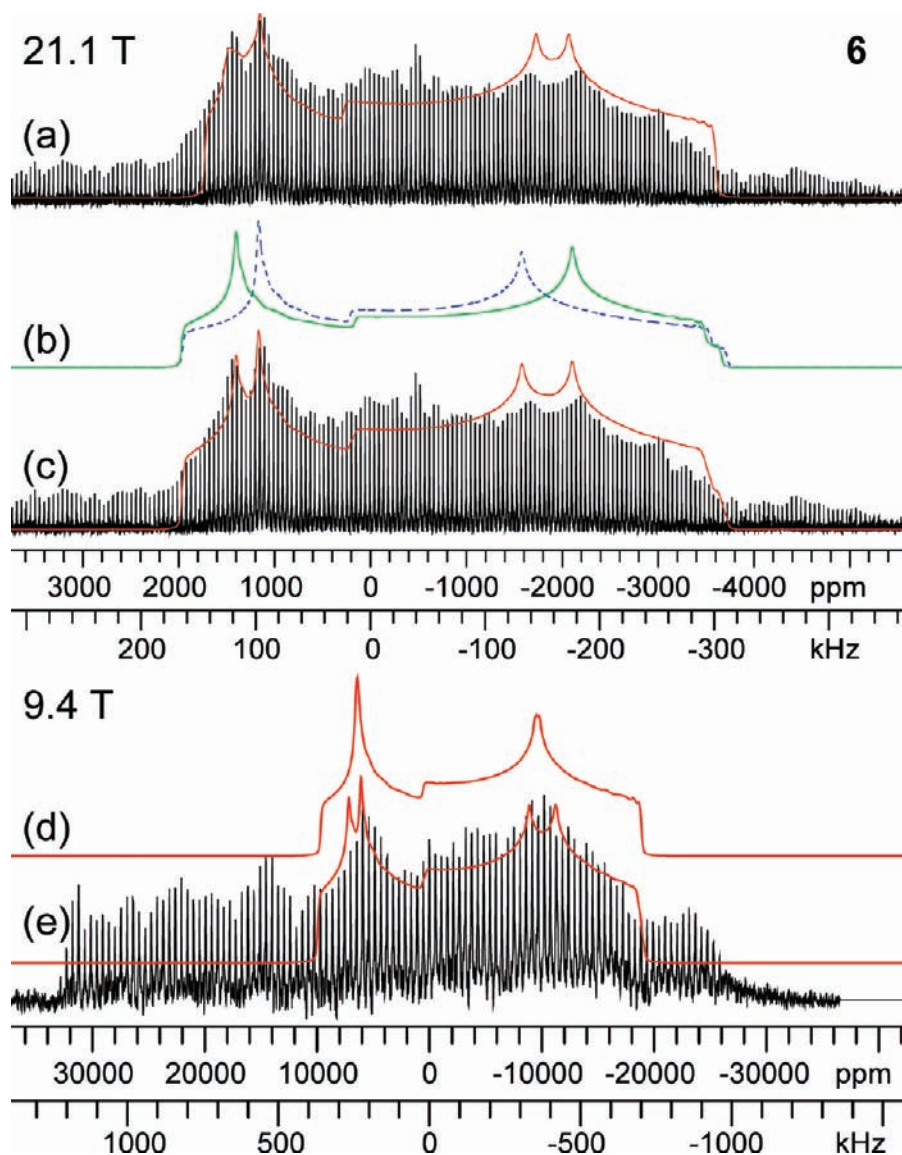
Figure 4. Static ^{91}Zr SSNMR spectra and analytical simulations of **6** [Ind$_2$ZrCl$_2$] acquired at fields of 21.1 T (top) and 9.4 T (bottom). (a) Analytical simulation employing a single site overlaid on the experimental WURST-QCPMG spectrum. (b) Deconvolution of the individual sites of the two site simulation. (c) Analytical simulation employing two-sites overlaid on the experimental WURST-QCPMG spectrum. (d) Simulation of the experimental pattern employing a single site. (e) Analytical simulation employing two sites overlaid on experimental piece-wise QCPMG spectrum. The satellite transitions of nearby $^{35/37}$Cl resonances are much more intense in the 9.4 T spectrum and obscure the ^{91}Zr signal.

for the other halogen complexes is obtained. Quantum chemical calculations employing atomic coordinates from the single-crystal XRD structure predict a large C_Q (vide infra) of ~30 MHz suggesting that our simulations are valid. **6** possesses Zr–Cl distances and Cl–Zr–Cl angles similar to those observed for Cp$_2$ZrCl$_2$ and **1**, suggesting that the large difference in C_Q must then be due to the asymmetry of the indenyl ligands. It has been noted that the two carbon atoms common to the five- and six-membered rings within the indenyl ligands possess much longer C–Zr bond lengths [average r(Zr–C) of 2.599 Å] than the Zr–C bond lengths of the three carbon atoms [average r(Zr–C) of 2.486 Å] exclusive to the five-membered ring.[98] The large asymmetry in Zr–Cp carbon atom bond lengths is not observed for the other complexes, suggesting that this is the most likely source of the large increase in C_Q for **6**.

Complexes **7** to **9** were investigated because of their roles in the olefin polymerization process (Scheme 1). In industrial olefin polymerization processes, a chlorinated form of the metallocene

precatalyst, such as Cp$_2$ZrCl$_2$, is reacted with an excess of the cocatalyst, MAO (10^2 to 10^4 equiv).[3,4,38] The reaction with MAO also leads to the formation of the monomethyl and dimethyl complexes, **7** and **8**. MAO also serves as an activator by further abstracting a methyl group from **8**, leading to a cationic complex, which is the active polymerization catalyst. In this case, complex **9** will serve as a mimic of the active catalyst.

The static ^{91}Zr NMR spectra of **7** seem to indicate the presence of two distinct Zr sites (Figure 5); however, a previously published single crystal XRD structure contains only one magnetically distinct Zr site.[99] An abnormally long Zr-methyl carbon distance [r(Zr–Me) = 2.36 Å] was observed in this structure, suggesting that the methyl and chlorine positions may be disordered.[99] We obtained a new single crystal XRD structure of **7**, which has been modeled with disordered methyl carbon and chlorine positions, resulting in two magnetically distinct Zr sites with uneven occupancies (see SI for CIF file). The new structure possesses a r(Zr–Me) of 2.227 Å (occupancy

Scheme 1. Reaction of Excess Amounts of Methylalumoxane (MAO) with a Catalyst Precursor (Cp₂ZrCl₂) Results in the Abstraction of the Chloride Ligands and Methylation of the Zirconium Center Leading to the Formation of **7** and **8**[a]
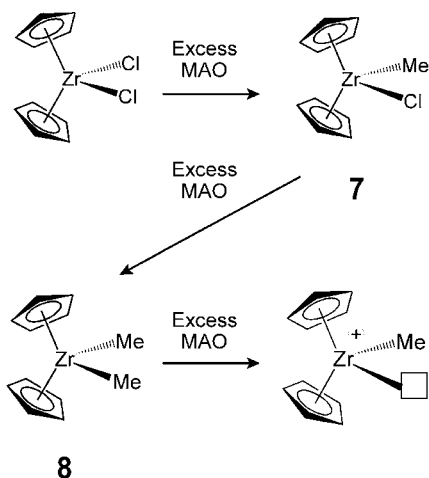
[a] Further abstraction of a methyl group by MAO results in a cationic zirconocene with a vacant coordination site (the active polymerization catalyst) and generation of an anionic methyl-MAO adduct.

of 0.616) and a $r(Zr-Me)$ of 2.176 Å (occupancy of 0.384) for the two distinct Zr sites. The latter distance seems unrealistically short and is probably a byproduct of limited resolution in the XRD experiments. Extensive characterization with both powder XRD, solution ^{13}C, ^{1}H and ^{91}Zr NMR and ^{13}C SSNMR experiments confirms the sample of **7** was of high purity (see SI, Figures S9–S14).

Simulations of the experimental spectra of **7** employing two sites of equal integrated intensity are shown in Figure 5. For both sites, $\delta_{iso} = 230$ ppm while values of Ω (900 and 1000 ppm) and C_Q (23.3 and 20.0 MHz) are similar in magnitude; however, the two sites have very distinct η_Q values (for site 1, $\eta_Q = 0.35$ and for site 2, $\eta_Q = 0.75$) and Euler angles, perhaps reflecting the uneven occupancies and slightly differing Zr environments indicated by the single-crystal structure. Simulated spectra at both fields possess low frequency discontinuities which are slightly more intense than those of the experimental spectra; even if the Euler angles and CS tensor parameters are freely varied, it is not possible to produce a fit of the 9.4 T spectrum which possesses a low frequency discontinuity of the appropriate intensity. We are uncertain of the origin of these discrepancies however, this spectrum is still useful for determining C_Q and η_Q. Hence, although there are large uncertainties associated with the experimental EFG and CS tensor parameters of **7**, the static ^{91}Zr SSNMR spectra still provide a useful "fingerprint" of this complex.

The static ^{91}Zr wideline QCPMG NMR spectrum of **8** exhibits a powder pattern with a breadth of 850 kHz at 9.4 T (Figure 6b), which yields a large C_Q of 27.9 MHz, and an η_Q value of 0.41, similar to that of Cp₂ZrCl₂. The Euler angles of **8** are found to be nearly identical to those of Cp₂ZrCl₂. A very large span of $\Omega = 1750$ ppm is obtained from simulations of the static spectra at both fields. The large C_Q value of **8** is consistent with the broad signal (full width half-height of 2530 Hz at 300 K) observed in the solution ^{91}Zr NMR spectrum of **8** by BHP. The difference of ~450 ppm in the δ_{iso} values of **8** and Cp₂ZrCl₂ in the solid-state is similar to the difference of ~500 ppm that is observed in solution ^{91}Zr NMR spectra (Figure S13 of the SI). Comparison of the crystal structures of Cp₂ZrCl₂ and **8** reveal that the Zr–Cp centroid (Zr–Cp$_{Cent}$) distances and Cp–Zr–Cp

angles are similar; however, the Zr–Me bond is much shorter than the Zr–Cl bond [$r(Zr-Me) = 2.28$ Å and $r(Zr-Cl) = 2.47$ Å].[99] The larger C_Q observed in **8** compared to that of Cp₂ZrCl₂ is likely due to the shorter bond lengths; however, the differences in the electronic structure of the two ligands also play an important role (this is further investigated in the theoretical section).

The static ^{91}Zr SSNMR spectrum of **9** at 21.1 T reveals an extremely large C_Q value of 39.0 MHz and an η_Q value of 0.76 (Figure 6c). This C_Q is significantly larger than those observed for **7** and **8** and slightly smaller than the value of 44.7 MHz measured for K₂ZrF₆, which is the largest $C_Q(^{91}Zr)$ measured by NMR to date.[71] The Zr-methyl carbon bond lengths are highly asymmetric for this complex: the methyl group which is bound solely to Zr possesses $r(Zr-Me) = 2.25$ Å, while the methyl group which bridges the adjacent Zr and B atoms possesses $r(Zr-Me) = 2.56$ Å.[125] Presumably, the large increase in C_Q for **9** arises due to the reduction in spherical symmetry about the zirconium center as compared to complex **8**. A sizable value of $\Omega = 1000$ ppm is also observed, although this is reduced in comparison to **8**. It is clear that ^{91}Zr solid-state NMR can readily distinguish the polymerization-active cationic zirconocenes, although samples containing a mixture of the species would give rise to complicated ^{91}Zr NMR spectra.

Theoretical Calculations. BHP have presented extensive quantum chemical calculations of ^{91}Zr EFG and CS tensors for a large series of zirconocenes.[84] They obtained the best results by using DFT methods, and basis sets similar to those employed herein. BHP estimated the magnitude of the largest component of the EFG tensor (V_{33}) based upon the observed linewidths of solution ^{91}Zr NMR spectra and were able to successfully reproduce the relative magnitudes of V_{33} with quantum chemical calculations. However, the V_{33} values calculated by BHP are ~2 to 3× greater in magnitude than those determined from the C_Q values obtained from our ^{91}Zr SSNMR spectra (see Table 3 footnote). The ^{91}Zr EFG tensor parameters obtained from SSNMR spectra are much more accurate than those obtained from solution ^{91}Zr NMR spectra, where under the assumptions of the extreme-narrowing limit, it is necessary to estimate the correlation time (τ_c) and η_Q.[84,126,127]

Calculations Using "Idealized" Cp Rings. A summary of results obtained from B3LYP calculations performed on atomic coordinates obtained from single crystal XRD structures is presented in Table 3. Extensive tests of Zr, Cl and Br basis sets were performed on Cp₂ZrCl₂ and **2** (Tables S9 and S10 of the SI). Regardless of the basis sets and methods employed, relatively poor agreement between the experimentally determined and calculated EFG tensor parameters, C_Q and η_Q, is generally observed when coordinates from single crystal X-ray structures are employed in the calculations for Cp₂ZrCl₂ and complexes **1** to **5** (Table 3). Examination of the individual crystal structures of the complexes reveals that there is a substantial variation in the interatomic carbon–carbon distances; for example, in Cp₂ZrCl₂ the C–C distances range from 1.364 to 1.414 Å. There are also deviations of the Cp rings from planarity, as indicated by torsional angles of four carbons in

(125) Guzei, I. A.; Stockland, R. A.; Jordan, R. F. *Acta Crystallogr. Sect. C-Cryst. Struct. Commun.* **2000**, *56*, 635–636.
(126) Harris, R. K., Quadrupolar Effects. In *Nuclear Magnetic Resonance Spectroscopy*; Longman Scientific & Technical: Essex, pp 131–141.
(127) Abragam, A., In *The Principles of Nuclear Magnetism*, Oxford University: New York, 1961; pp 264–353.
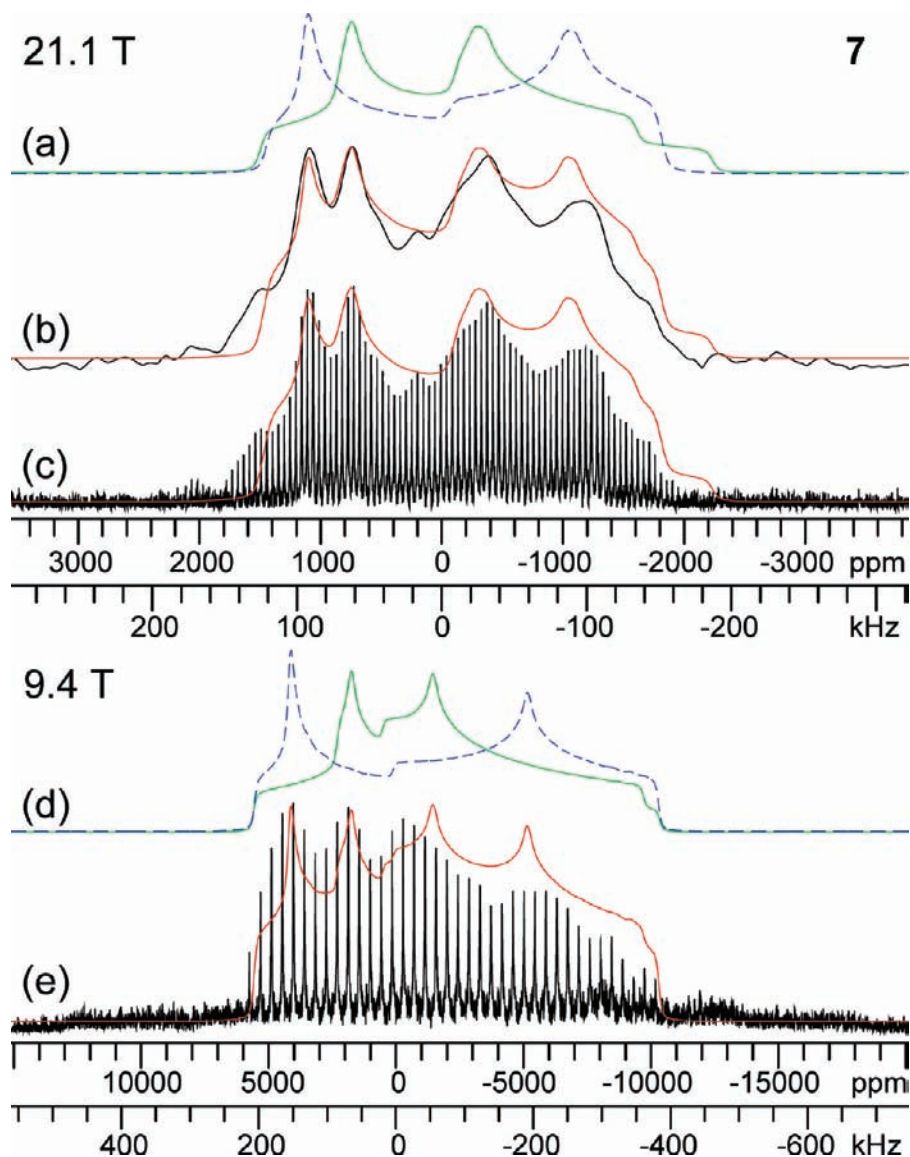
Figure 5. Static solid-state ^{91}Zr NMR spectra of **7** [Cp$_2$ZrMeCl] acquired with the WURST-QCPMG sequence at fields of 21.1 T (top) and 9.4 T (bottom). (a) Deconvolution of the individual sites employed in the two site simulation. (b) Two site analytical simulation (red trace) overlaid on the experimental spectrum formed by time domain coaddition of the echoes in the WURST-QCPMG echo train. (c) Two site analytical simulation overlaid on the experimental WURST-QCPMG spikelet spectrum. (d) Deconvolution of the individual sites employed in the two site simulation. (e) Two site analytical simulation (red trace) overlaid on the experimental piece-wise WURST-QCPMG spikelet spectrum.

the Cp rings. Distortions of up to 2.19° are observed in the crystal structure of Cp$_2$ZrCl$_2$ (this is typical of torsional angles observed in the other complexes). For this reason, calculations with "idealized" Cp rings were attempted. In these calculations, the crystallographically refined Cp ring structures have been replaced with perfectly flat Cp rings (0° torsional angles) with all C−C distances set to 1.40 Å and C−C−C internal angles of 108°. The crystallographically determined Zr−Cp$_\text{Cent}$ distances have been retained.

Calculations which employ such idealized Cp rings lead to significantly reduced V_{33} and C_Q values for Cp$_2$ZrCl$_2$, **1**, **2**, and **3**, and yield much better agreement with experimental values of C_Q (Table 3 and Tables S11 and S12 of the SI). All of these complexes possess small V_{33} values, and minor deviations in the Cp′ carbon atom positions would be expected to reduce the symmetry around the Zr atom and give rise to larger EFGs; however, it is somewhat surprising to observe that minor deviations in the positions of the carbons within the Cp rings

can lead to 2- to 4-fold differences in the magnitude of V_{33}. For complexes **4** and **5**, calculations on structures with ideal Cp rings lead to only slight differences in the calculated EFG and CS tensor parameters. Complexes **7**, **8**, and **9** feature coordination by methyl ligands and possess values of C_Q greater than 20 MHz. The use of ideal Cp rings leads to changes in calculated values of C_Q by 3 to 4 MHz compared to calculations utilizing X-ray coordinates for Cp carbon atoms. This suggests that the large values of V_{33} observed for **7**, **8**, and **9** relative to those of the halogenated zirconocenes mainly arise from the presence of the methyl ligands coordinated to Zr rather than from differences in the Cp carbon positions (vide infra). Calculations utilizing X-ray coordinates for Cp′ carbon atoms and the idealized Cp′ rings yield very similar CS tensor parameters for all complexes. In summary, calculations utilizing idealized Cp′ rings with Zr−Cp′$_\text{Cent}$ distances determined from X-ray structures should be used for quantum chemical calculations of ^{91}Zr EFG tensor parameters of zirconocenes.
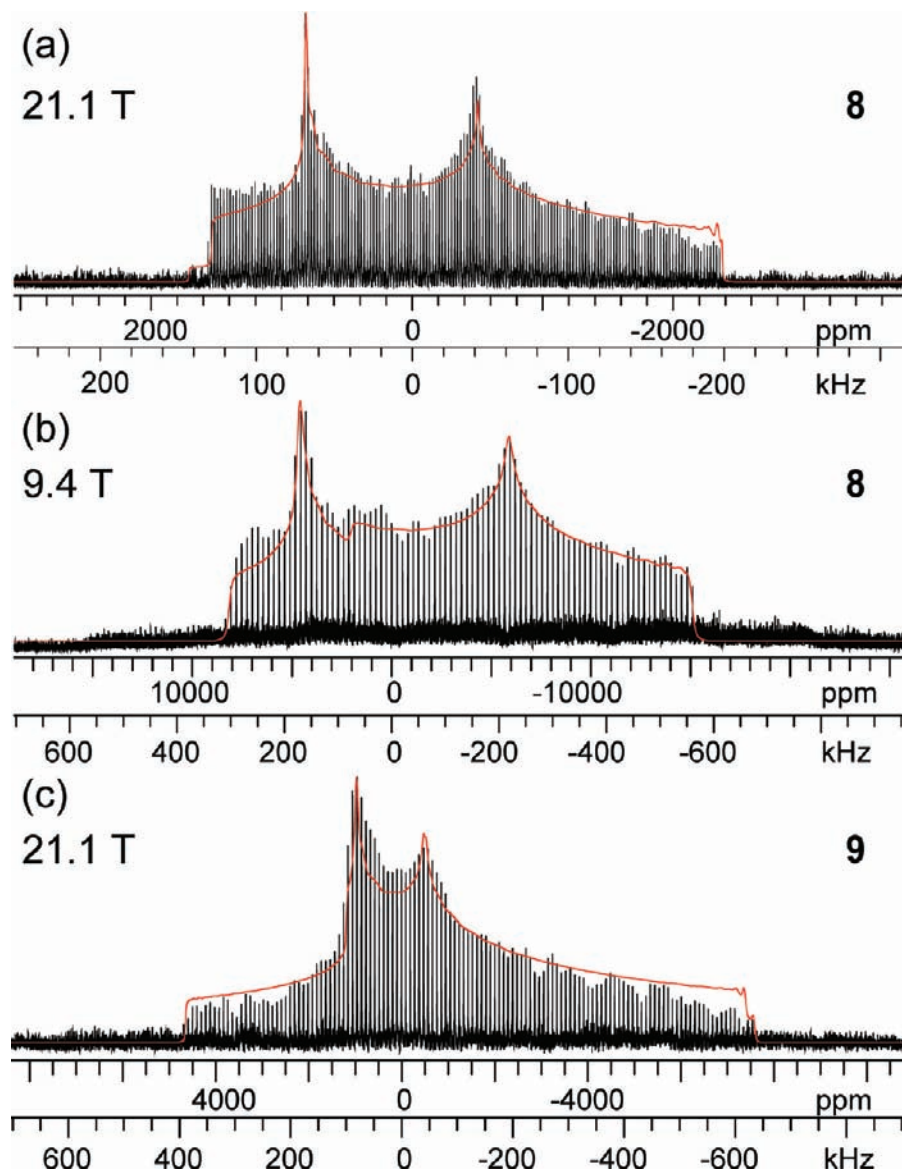
Figure 6. Static ^{91}Zr SSNMR spectra of **8** [Cp$_2$ZrMe$_2$] and **9** [Cp$_2$ZrMe][MeB(C$_6$F$_5$)$_3$]. Analytical simulations (red traces) overlaid on the experimental WURST-QCPMG spectra of **8** acquired at fields of (a) 21.1 T and (b) 9.4 T. (c) Analytical simulation (red trace) overlaid on the experimental WURST-QCPMG spectrum of **9** acquired at a field of 21.1 T. Experiments on **9** were attempted at 9.4 T, however no signal could be observed. This is due to the large breadth of the central transition powder pattern at this field.

Structural Anomalies and Calculation of NMR Tensors. Calculations on **1** employing atomic coordinates from the single-crystal X-ray structure[113] show poor agreement with experimental values, regardless of whether X-ray or idealized Cp* rings were utilized. BHP used atomic coordinates from the previously published crystal structure of (Me$_4$EtCp)$_2$ZrCl$_2$[128] to construct a model of **1**; with this approach, they observed good agreement between the calculated and experimental values of δ_{iso}.[84] We have taken a similar approach, and our calculations yield ^{91}Zr NMR tensor parameters in excellent agreement with experimental values (Table 3). The only notable differences evident in the crystal structures of **1** and (Me$_4$EtCp)$_2$ZrCl$_2$ are the Cp$'_{Cent}$−Zr−Cp$'_{Cent}$ angles (130.9° and 137.0°, respectively, Table 2). The success of these calculations suggests that there may be an error in the previously published crystal structure of **1**.

The crystal structure of **2** has two crystallographically distinct Zr atoms (sites 1 and 2); in addition, site 2 has two Cp ring conformations. There is a significant variation in calculated C_Q and η_Q values for the two distinct Cp ring conformations of site 2; however, the Zr−Cp$_{Cent}$ distance of conformation 2 is significantly longer than the other distances within the structure, and casts doubt on the accuracy of the crystal structure. This suggests that the two resonances observed in the MAS ^{91}Zr NMR spectrum arise from the two crystallographically distinct Zr sites, rather than from distinct conformations of the Cp rings.

Simulations of the static ^{91}Zr SSNMR spectra of **7** required two sites with disparate values of η_Q in order to produce reasonable fits of the experimental spectra. Calculations on a model based on our new crystal structure (which indicates that the Me and Cl positions are disordered) indicate that η_Q does not vary between the two sites; however, calculations on two cluster models (Figure S15 of the SI) suggest that long-range electrostatic interactions arising from neighboring molecules may influence the EFG tensor parameters. In both cases, the central molecule of the cluster corresponds to site 2 (i.e.,

Table 3. Experimental and Calculated ^{91}Zr CS and EFG Tensor Parameters Determined with the B3LYP Method and [6s3p3d] Basis Set on Zr[a]

compound	site/structure	V_{33} (a.u.)[b]	C_Q (MHz)[c]	η_Q	δ_{iso} (ppm)[d]	Ω (ppm)[e]	κ [e]
Cp$_2$ZrCl$_2$	experimental site 1	0.150	6.2	0.18	21	350	−0.7
	experimental site 2	0.157	6.5	0.30	21	340	−0.6
	1/X-ray [f]	−0.249	−10.3	0.22	35	499	−0.5
	2/X-ray [f]	−0.262	−10.8	0.19	18	511	−0.6
	1/ideal Cp[f]	−0.134	−5.6	0.22	21	454	−0.6
	2/ideal Cp	−0.147	−6.1	0.30	21	456	−0.6
Cp*$_2$ZrCl$_2$ **1**	experimental	0.063	2.6	0.22	208	235	−0.8
	1/X-ray	0.137	5.7	0.75	178	335	0.7
	1/ideal Cp	−0.239	−9.9	0.22	384	352	0.8
	1/X-ray (Me$_4$EtCp)[g]	−0.117	−4.8	0.56	179	251	−0.8
	1/ideal (Me$_4$EtCp)[g]	0.072	3.0	0.23	164	286	−0.5
Cp$_2$ZrBr$_2$ **2**	experimental	0.058	2.4	0.40	127	550	−0.6
	1/X-ray	−0.151	−6.2	0.86	132	811	−0.6
	2/X-ray conf. 1	0.137	5.6	0.67	136	728	−0.7
	2/X-ray conf. 2	0.030	1.2	0.58	158	728	−0.6
	1/ideal Cp	−0.032	−1.3	0.57	156	700	−0.7
	2/ideal Cp conf. 1	−0.038	−1.6	0.39	142	692	−0.7
	2/ideal Cp conf. 2	−0.049	−2.0	0.16	162	707	−0.7
(Me$_3$SiC$_5$H$_4$)$_2$ZrBr$_2$ **3**	experimental	0.114	4.7	0.88	154	−	−
	1/X-ray	−0.169	−7.0	0.76	132	634	−0.9
	1/ideal Cp	0.107	4.4	0.56	118	589	−1.0
O(Me$_2$SiC$_5$H$_4$)$_2$ZrBr$_2$ **4**	experimental	0.061	2.5	0.68	143	620	−0.8
	1/X-ray	0.098	4.0	0.70	143	707	−0.7
	1/ideal Cp	−0.104	−4.3	0.54	133	692	−0.7
(1,3-C$_5$H$_3$)(SiMe$_2$OSiMe$_2$)$_2$(1,3-C$_5$H$_3$)ZrBr$_2$ **5**	experimental	0.095	3.9	0.25	163	530	−0.6
	1/X-ray	−0.094	−3.9	0.88	114	620	−0.7
	1/ideal Cp	−0.109	−4.5	0.31	98	637	−0.5
Ind$_2$ZrCl$_2$ **6**	experimental site 1	0.779	32.0	0.25	60	200	−0.3
	experimental site 2	0.748	30.7	0.38	56	200	−0.3
	1/X-ray	−0.729	−30.1	0.08	64	332	−0.3
Cp$_2$ZrMeCl **7**	experimental site 1	0.563	23.3	0.35	230	900	−0.6
	experimental site 2	0.484	20.0	0.75	230	1000	0.8
	1/X-ray	0.535	22.1	0.23	325	1205	−0.6
	1/ideal Cp	0.477	19.7	0.07	334	1194	−0.6
	1/new X-ray[h]	0.870	36.0	0.18	318	1287	−0.5
	2/new X-ray	0.811	33.6	0.09	329	1259	−0.6
	1/new ideal Cp	0.875	36.2	0.03	317	1250	−0.5
	2/new ideal Cp	0.731	30.2	0.02	329	1247	−0.5
Cp$_2$ZrMe$_2$ **8**	experimental	0.677	27.9	0.41	475	1750	−0.9
	1/X-ray	−0.714	−29.5	0.20	622	1873	−0.9
	1/ideal Cp	−0.615	−25.4	0.29	624	1842	−1.0
[Cp$_2$ZrMe][MeB(C$_6$F$_5$)$_3$] **9**	experimental	0.946	39.0	0.76	350	1000	0.2
	1/X-ray	−0.887	−36.7	0.96	325	1066	−0.4
	1/ideal Cp	−0.952	−39.4	0.81	334	1049	−0.4

[a] Additional computational results can be found in Tables S9 to S13 of the SI. See text for details on basis sets used in the calculations. The 6s3p3d basis set was used for Zr, cc-pVDZ for Cl and 6-311G** on Br. [b] See the experimental section for details on the basis sets used on other atoms. [c] Only the magnitude of C_Q can be measured experimentally. For definitions of all NMR parameters refer to Table 1. [d] The theoretical values of δ_{iso} were determined by comparison to the magnetic shielding values calculated from calculations on Cp$_2$ZrCl$_2$ which utilized ideal Cp rings and the corresponding method and basis sets (Table S2 of the SI). The equation used was, $\delta_{iso} = \sigma_{iso}(\text{Cp}_2\text{ZrCl}_2 \text{ ideal Cp}) - \sigma_{iso}(x) + 21$ ppm. [e] Defined in Table 1. [f] "X-ray" refers to calculations with Cp carbon atom coordinates determined from single crystal XRD structures. "ideal Cp" refers to calculations where idealized Cp carbon atom coordinates have been used. See text for details. [g] These calculations employ coordinates from the single crystal XRD structure of (Me$_4$EtCp)$_2$ZrCl$_2$, where the Et groups have been replaced with Me groups. [h] These calculations employ coordinates from the single crystal XRD strucutre of Cp$_2$ZrMeCl presented in this work.

$r(\text{Zr}-\text{Me}) = 2.23$ Å and $r(\text{Zr}-\text{Cl}) = 2.51$ Å). In cluster 1, all neighboring units correspond to site 2 of the single crystal XRD structure (i.e., all neighboring units possess $r(\text{Zr}-\text{Me}) = 2.23$ Å and $r(\text{Zr}-\text{Cl}) = 2.51$ Å). In cluster 2, four of the neighboring units correspond to site 1 (i.e., $r(\text{Zr}-\text{Me}) = 2.18$ Å and $r(\text{Zr}-\text{Cl}) = 2.51$ Å). The four neighboring units that were changed were chosen because their Me or Cl ligands were directed toward the central molecule of the cluster. Calculations on both clusters reveal similar values of C_Q; however, values of η_Q are 0.66 and near zero for clusters 1 and 2, respectively. This strongly suggests that variations in EFG tensor parameters can be altered by the presence of neighboring molecules.

Tensor Orientations. The theoretically obtained ^{91}Zr EFG and magnetic shielding (MS) tensor orientations within the molecular frames are now discussed (Figures 7 and 8). Euler angles extracted from the quantum chemical calculations are shown in Table 4. The good agreement observed between the calculated and experimentally determined EFG and CS tensor parameters suggests that the calculated tensor orientations are valid. For all complexes, the least shielded component of the MS tensor (σ_{11}) is oriented in a direction approximately perpendicular to the X−Zr−X plane (X = Me, Cl, Br). Nuclear deshielding in this direction arises from magnetic dipole induced mixing of occupied and virtual molecular orbitals (MOs) within the X−Zr−X plane [i.e., virtual MOs of high Zr d atomic orbital character and occupied Zr−X σ- (X = CH$_3$, Cl, Br) and π-bonding (X = Cl, Br) MOs]. This is consistent with previous Hückel MO calculations on bent metallocene complexes by Lauher and Hoffman, which show that Zr−X σ and π MOs are the highest occupied MOs in these complexes, and that their
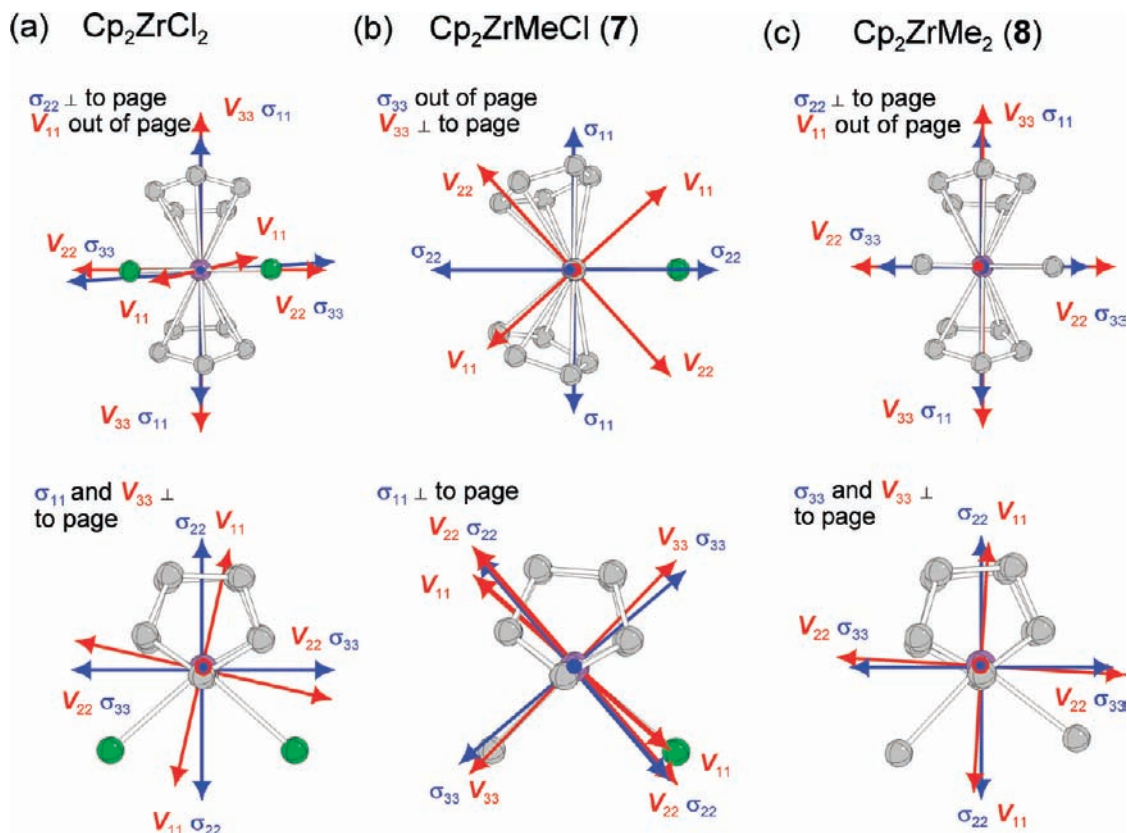
Figure 7. Theoretical ^{91}Zr EFG and MS tensor orientations in the molecular frames of (a) Cp_2ZrCl_2, (b) **7** [$Cp_2ZrMeCl$], and (c) **8** [Cp_2ZrMe_2]. All tensor orientations are taken from the calculations which employ idealized Cp rings. The tensor orientation for Cp_2ZrCl_2 has been taken from site 1. The tensor orientation for $Cp_2ZrMeCl$ has been taken from calculations on site 2 of the new structure (see text for full explanation).

electron densities are largely concentrated within or about the X−Zr−X plane.[129] The only exception we note is **6**, where a significant deviation away from orthogonality is observed (σ_{11} forms a torsional angle of ∼78° with the Cl−Zr−Cl plane); this may arise from the positioning of the indenyl rings.

The tensor orientations for the series of complexes found in Scheme 1 (Cp_2ZrCl_2 and **7−9**) are discussed first. Quantum chemical calculations predict similar orientations of EFG tensors for Cp_2ZrCl_2 (Figure 7a) and **8** (Figure 7c): V_{11} and V_{22} lie approximately within the X−Zr−X (X = Me, Cl) plane and V_{33} is directed toward the Cp rings forming torsional angles with the X−Zr−X plane of 88.4° and 90.3° for X = Me and X = Cl, respectively. The tensor orientations presented for Cp_2ZrCl_2 are similar to those previously reported by our research group.[54] The EFG orientations in Cp_2ZrCl_2 and **8** are consistent with experimental values of η_Q being closer to 0 than 1, which indicate that V_{33} is the distinct component of the EFG tensor. For both complexes, the least shielded component of the MS tensor (σ_{11}) is approximately colinear with the largest component of the EFG tensor (V_{33}), and the most shielded component (σ_{33}) is predicted to lie in the X−Zr−X plane near V_{22}; this is consistent with the Euler angles of $\alpha \approx \beta \approx 90°$ obtained from simulations of the static ^{91}Zr NMR spectra.

The EFG tensor orientation in **7** is distinct from that of the other complexes: V_{33} is oriented such that it is coincident with the Zr−Me bond, while V_{11} and V_{22} make angles of approximately 45° with respect to the Me−Zr−Cl plane (Figure

7b, top). The orientation of V_{33} along the Zr−Me bond suggests that the increase in C_Q observed for **7** compared to that of Cp_2ZrCl_2 can be attributed to the asymmetry of the Zr−Me and Zr−Cl bonds. Unfortunately, given the uncertainty regarding the simulations of the static NMR spectra of **7**, it is difficult to compare experimental and calculated Euler angles, although a calculated value of β near zero is distinct from the other complexes. The EFG and MS tensor orientation for **9** are shown in Figure 8a. The η_Q value near 1 is consistent with the orientation of V_{11} toward the Cp rings, with V_{33} and V_{22} oriented near the Zr−Me carbon bonds (V_{33} is directed toward the bridging methyl group). This suggests that the large C_Q observed for this complex results in part from the asymmetry of the Zr−Me carbon bond lengths (vide infra).

Complexes **1−5** are all characterized by small C_Q values (less than that of Cp_2ZrCl_2) and η_Q values which vary from near 0 to near 1. For all of these complexes, V_{33} is oriented such that it is contained within or near the X−Zr−X plane (Figure 8 b−e, orientations for **3** not shown), although the direction of V_{33} within this plane is variable and seems to be uncorrelated to the predicted sign of C_Q or value of η_Q. We posit that this is because when V_{33} is small, subtle differences in ligand positions can result in completely different EFG tensor orientations. In complex **6**, V_{33} is directed toward the carbon atoms which are common to the five- and six-membered rings of the indenyl ligands (Figure 8f). This supports the notion that the large increase in C_Q for **6** as compared to Cp_2ZrCl_2 can be attributed to the asymmetric binding of the indenyl ligands (vide supra).

EFG Parameters and Bond Length Variation. Finally, due to the importance of Cp_2ZrCl_2 and complexes **7−9** in olefin

(128) Kurz, S.; Heyhawkins, E. *Z. Kristallogr.* **1993**, *205*, 61–67.
(129) Lauher, J. W.; Hoffmann, R. *J. Am. Chem. Soc.* **1976**, *98* (7), 1729–1742.
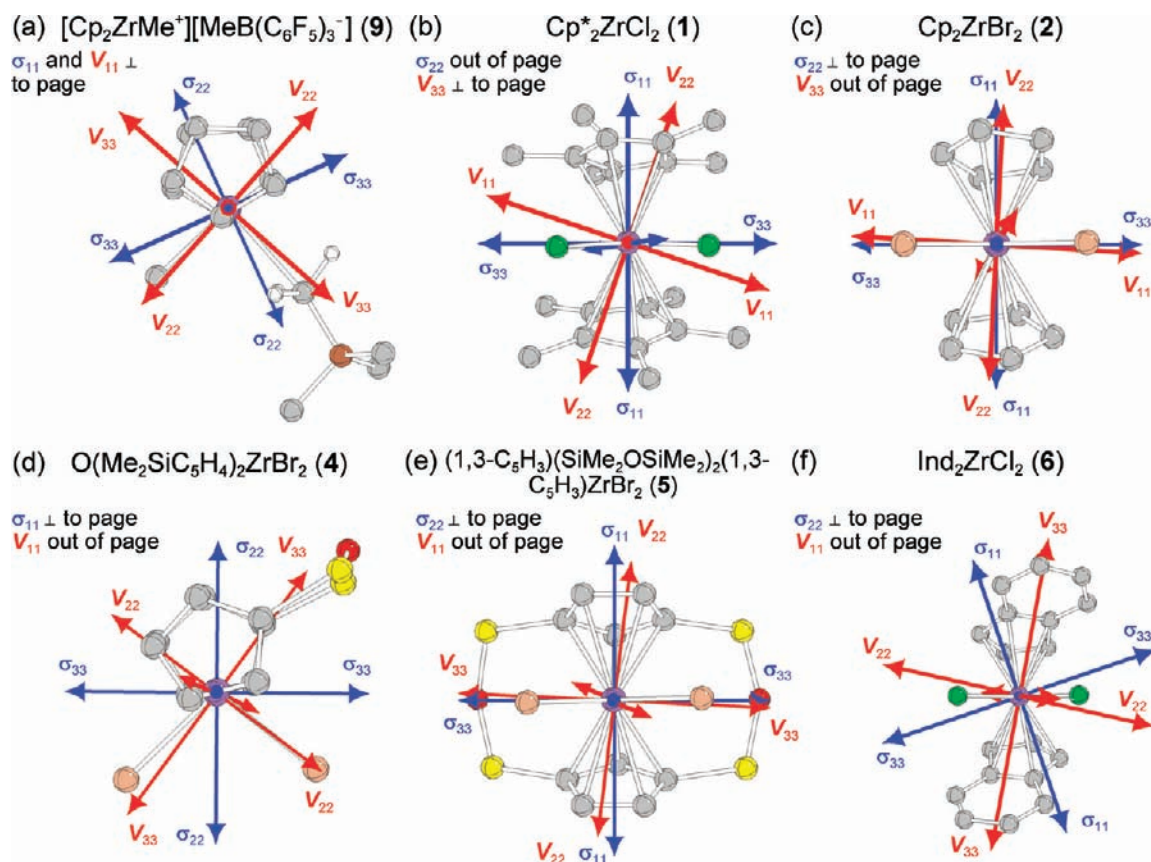
Figure 8. Theoretical ^{91}Zr EFG and MS tensor orientations in the molecular frames of (a) **9**, (b) **1** [Cp*$_2$ZrCl$_2$], (c) **2** [Cp$_2$ZrBr$_2$], (d) **4** [O(Me$_2$SiC$_5$H$_4$)$_2$ZrBr$_2$], (e) **5** [(1,3-C$_5$H$_3$)(SiMe$_2$OSiMe$_2$)$_2$(1,3-C$_5$H$_3$)ZrBr$_2$], and (f) **6** [Ind$_2$ZrCl$_2$]. All tensor orientations are taken from the calculations which employ idealized Cp rings. The tensor orientation for complex **2** has been taken from site 1.

Table 4. Experimentally Determined and Calculated Euler Angles[a]

compound	method/structure	α (deg)	β (deg)	γ (deg)
Cp$_2$ZrCl$_2$	experiment site 1	90(35)	86(10)	2(10)
	experiment site 2	90(35)	86(10)	3(10)
	site 1 ideal Cp	103	89	1
	site 2 ideal Cp	108	88	−1
Cp*$_2$ZrCl$_2$ **1**	experiment	20(40)	90(25)	90(10)
	ideal (Me$_4$EtCp)	−20	82	90
Cp$_2$ZrBr$_2$ **2**	experiment	40(90)	0(90)	0(90)
	site 1 ideal Cp	1	82	103
O(Me$_2$SiC$_5$H$_4$)$_2$ZrBr$_2$ **4**	experiment	40(20)	90(15)	35(40)
	ideal Cp	98	56	−91
(1,3-C$_5$H$_3$)(SiMe$_2$OSiMe$_2$)$_2$(1,3-C$_5$H$_3$)ZrBr$_2$ **5**	experiment	40(20)	30(15)	85(10)
	ideal Cp	17	20	87
Ind$_2$ZrCl$_2$ **6** (two site fit, site 1)	experiment	80(60)	60(40)	4(60)
Ind$_2$ZrCl$_2$ **6** (two site fit, site 2)	experiment	80(60)	60(40)	4(60)
	ideal Cp	80	60	0
Cp$_2$ZrMeCl **7** (site 1)	experiment	5(70)	15(45)	85(70)
Cp$_2$ZrMeCl **7** (site 2)	experiment	80(40)	20(20)	5(40)
	site 2 ideal Cp new struct.	36	6	97
Cp$_2$ZrMe$_2$ **8**	experiment	80(40)	90(5)	0(5)
	ideal Cp	93	89	1
[Cp$_2$ZrMe][MeB(C$_6$F$_5$)$_3$] **9**	experiment	90(10)	80(15)	86(40)
	ideal Cp	−90	63	90

[a] Euler angle conventions are specified in the experimental section.

polymerization catalysis, it is important to further probe the origin of the large differences observed and predicted in the values of C_Q and η_Q in this series. We have calculated the EFG tensor parameters for structures with variable Zr−X (X = Cl, Me) bond lengths, since all of these complexes possess similar Cp$_{Cent}$−Zr bond lengths, Cp$_{Cent}$−Zr−Cp$_{Cent}$ angles and X−Zr−X

angles (Table 2). We have performed calculations on Cp$_2$ZrCl$_2$ and **8** where the Zr−X bond lengths are *symmetrically short-ened*. A full discussion of these results can be found in the SI. From these calculations (Figure 9a) it is clear that the large increase in C_Q observed for **8** can be attributed to the much shorter r(Zr−Me) in **8** (2.28 Å) as compared to the relatively
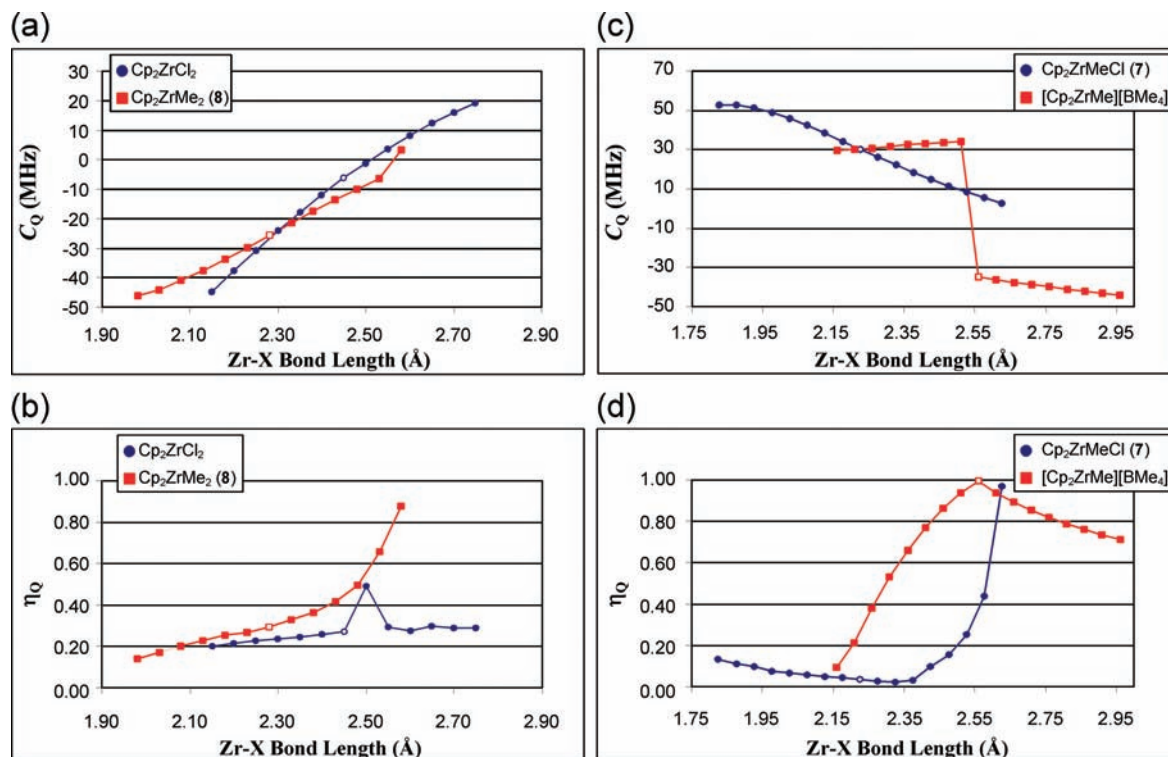
Figure 9. Values of ^{91}Zr EFG tensor parameters obtained from B3LYP calculations on structures with variable Zr−Cl and Zr−Me carbon bond lengths. The bond lengths were varied in increments of 0.05 Å. Calculated (a) C_Q and (b) η_Q values when both of the Zr−X (X = Cl, Me) bond lengths in Cp$_2$ZrCl$_2$ and **8** [Cp$_2$ZrMe$_2$] are varied. Calculated (c) C_Q and (d) η_Q values when the Zr−Me bond length of **7** [Cp$_2$ZrMeCl] is varied and when the bridging Zr−Me bond length of [Cp$_2$ZrMe][BMe$_4$] is varied. The model complex, [Cp$_2$ZrMe][BMe$_4$], was created by replacing the three pentafluorophenyl groups of **9** with Me groups. Crystallographic bond lengths are marked with open circles and squares. Atomic coordinates with idealized Cp rings were employed for all calculations. Coordinates from site 1 of Cp$_2$ZrCl$_2$ and site 2 of **7** of the respective crystal structures were employed.

long r(Zr−Cl) in Cp$_2$ZrCl$_2$ (2.45 Å), although, the different bonding characteristics of the Cl and Me ligands will also contribute to the magnitude of V_{33}.

Since there is some uncertainty associated with the crystallographically determined values of r(Zr−Me) for **7** (vide supra), EFG tensor parameter calculations were performed on a model structure of **7** in which r(Zr-Me) was altered, while r(Zr−Cl) was held constant at its crystallographically determined value (Figure 9c,d). These calculations reveal that the value of η_Q is relatively constant when r(Zr−Me) is less than 2.48 Å. This suggests that the high η_Q site observed in the static ^{91}Zr SSNMR spectra is not arising from disorder in the position of the methyl group, but rather from longer range electrostatic interactions (vide supra). Finally, in order to probe the origins of the large C_Q and high η_Q observed for **9**, EFG tensor parameters were calculated for a model complex which is analogous to **9**, [Cp$_2$ZrMe][BMe$_4$]. The r(Zr−Me) of the bridging Me group was then varied (the BMe$_3$ fragment was also moved by the same amount), while the terminal r(Zr−Me) was fixed at the crystallographic distance observed for **9** (2.25 Å). These calculations suggest that the large value of C_Q observed for **9** and the η_Q values close to 1 arise from unequal Zr−Me bond lengths for the bridging and terminal methyl groups. Comparison to calculated values of C_Q for **8** also suggest that when the hydrogen atoms of the bridging Me group are directed toward the Zr center, an increase in $|C_Q|$ will also occur.

Conclusions

The use of ^{91}Zr SSNMR and quantum mechanical calculations has allowed for the examination of the ^{91}Zr quadrupolar and

chemical shift interactions in zirconocenes possessing Cp ligands of varying substitution patterns and different heteroligands (i.e., Cl, Br, Me). In general, halide complexes are characterized by small C_Q values, while the coordination of methyl ligands leads to larger C_Q values. Isotropic ^{91}Zr chemical shifts are seen to parallel those previously observed in solution ^{91}Zr NMR spectra, and allow for variations in the Cp ring substitution patterns as well as the types of heteroligands coordinated to the metal to be differentiated. CSA is observed to be very sensitive to the nature of the heteroligand; Ω is seen to increase for the ligand series Cl, Br, and Me, affording another parameter which allows for insight into zirconocene structure and bonding. Methods for the accurate calculation of ^{91}Zr EFG and MS tensor parameters have been identified, and visualization of the tensor orientations within the molecular frames allows for the origins of the NMR interactions to be rationalized. In future investigations, quantum chemical calculations on model systems developed from a combination of known structural models and geometrical optimization and energy minimization should prove invaluable for investigating complex zirconocene systems of unknown structure.

The purpose of studying compounds **3**−**5** was to mimic the structures of zirconocene species before (**3**) and after (**4** and **5**) chemisorption to surface materials via the ancillary functional groups of the Cp ligands. Cp$_2$ZrCl$_2$ and complexes **7**−**9** were studied in order to demonstrate that ^{91}Zr SSNMR can differentiate the key intermediates that result from the reaction of MAO with a precatalyst (Cp$_2$ZrCl$_2$), which may allow for the interactions between MAO and zirconocenes to be probed for both homogeneous and heterogeneous catalysts. The combina-

tion of ^{91}Zr and ^{35}Cl SSNMR[57] and quantum chemical calculations should allow for the structure of immobilized zirconocenes with ambiguous structures to be probed, which will be crucial for the future development of industrially viable heterogeneous olefin polymerization catalysts.

The acquisition of ^{91}Zr NMR spectra of heterogeneous catalyst systems will prove challenging due to the dilution of the ^{91}Zr nuclei (typical heterogeneous catalysts are 0.5−5% Zr by mass). For crystalline samples which possessed narrow CT powder patterns (e.g., Cp_2ZrCl_2) it was possible to acquire static spectra in a matter of minutes at 21.1 T with standard echo sequences, suggesting that the acquisition of ^{91}Zr SSNMR spectra of heterogeneous catalysts featuring narrow resonances is feasible with standard techniques. However, if the halide ligands are replaced during immobilization and/or the metallocene structure is significantly altered, a large increase in the breadth of the NMR pattern is expected (compare spectra of Cp_2ZrCl_2 and **8**). The combination of WURST-QCPMG and ultrahigh magnetic fields allows for the acquisition of ^{91}Zr UW SSNMR spectra of **7**, **8**, and **9** in total experimental times of 4.6, 1.1, and 9.1 h, respectively. Therefore, the acquisition of solid-state ^{91}Zr NMR spectra of heterogeneous catalysts possessing broad ^{91}Zr resonances would be a considerable challenge. In these cases, ^{91}Zr isotopic enrichment and/or cryogenic temperatures in combination with ^{1}H cross-polarization QCPMG (CP/QCPMG) pulse sequences would be necessary in order to obtain high S/N NMR spectra,[47,48,130] as demonstrated by Ellis and Lipton for SSNMR studies of quadrupolar metal nuclei present in low concentrations in the active sites of metalloproteins.[131−133]

Supporting Information Available: Details on the syntheses of complexes, detailed descriptions of single crystal X-ray diffraction experiments and crystallographic information files (CIF) for complexes **4**, **5**, and **7**, additional quantum chemical calculation results, powder X-ray diffraction patterns, solution ^{1}H, ^{13}C, and ^{91}Zr NMR spectra, and a complete list of authors for Gaussian 03 (ref 97). This material is available free of charge via the Internet at http://pubs.acs.org.

JA107749B

(130) Ellis, P. D.; Lipton, A. S., Low-temperature solid-state NMR spectroscopy. A strategy for the direct observation of quadrupolar nuclides of biological interest. In *Annual Reports on NMR Spectroscopy*, 2007; Vol. 60, pp 1−38.

(131) Lipton, A. S.; Heck, R. W.; Primak, S.; McNeill, D. R.; Wilson, D. M.; Ellis, P. D. *J. Am. Chem. Soc.* **2008**, *130* (29), 9332–9341.

(132) Lipton, A. S.; Heck, R. W.; de Jong, W. A.; Gao, A. R.; Wu, X. J.; Roehrich, A.; Harbison, G. S.; Ellis, P. D. *J. Am. Chem. Soc.* **2009**, *131* (39), 13992–13999.

(133) Lipton, A. S.; Heck, R. W.; Hernick, M.; Fierke, C. A.; Ellis, P. D. *J. Am. Chem. Soc.* **2008**, *130* (38), 12671–12679.